

Hydrothermal Plume Dynamics on Europa: Implications for Chaos Formation

Jason C. Goodman

Department of Geophysical Sciences, University of Chicago

Geoffrey C. Collins

Department of Physics and Astronomy, Wheaton College, Norton, MA

John Marshall

Department of Earth, Atmospheric, and Planetary Sciences, Massachusetts

Institute of Technology

Raymond T. Pierrehumbert

Department of Geophysical Sciences, University of Chicago

Corresponding Author: Jason C. Goodman, 5731 S. Ellis Ave., University of Chicago, Chicago,
IL 60637, <goodmanj@uchicago.edu>

Abstract.

Hydrothermal plumes may be responsible for transmitting tidally-generated heat from Europa's rocky interior through a liquid ocean to the base of its ice shell. This process has been implicated in the formation of chaos regions and lenticulae by melting or exciting convection in the ice layer. In contrast to earlier work, we argue that Europa's ocean should be treated as an unstratified fluid. We have adapted and expanded upon existing work describing buoyant plumes in a rotating, unstratified environment: we discuss the scaling laws governing the flow and geometry of plumes on Europa, and perform a laboratory experiment to obtain scaling constants and to visualize plume behavior in a Europa-like parameter regime. We predict that hydrothermal plumes on Europa are of a lateral scale (at least 25-50 km) comparable to large chaos regions; they are too broad to be responsible for the formation of individual lenticulae. Plume heat fluxes ($0.1-10 \text{ W/m}^2$) are too weak to allow complete melt-through of the ice layer. Current speeds in the plume (3-8 mm/s) are much slower than indicated by previous studies. The observed movement of ice rafts in the Conamara Chaos region is unlikely to be driven by such weak flow.

1. Introduction

Observational evidence for the existence of a liquid water layer beneath Europa’s icy surface is accumulating rapidly [*Pappalardo et al.*, 1999a; *Showman and Malhotra*, 1999]. Spacecraft gravitational studies indicate a low-density layer of water and/or ice between 80 and 170 km thick [*Anderson et al.*, 1998]. Magnetometer measurements [*Kivelson et al.*, 2000; *Zimmer and Khuruna*, 2000], require the presence of a layer of conductive material, most likely saline water, near the surface.

A large number of geological features on Europa’s surface can be explained by the presence of a liquid layer: see [*Pappalardo et al.*, 1999a] for a review. Europa’s surface shows few large craters, implying a young (~ 50 Ma), geologically-active surface [*Zahnle et al.*, 1998]. The orientation of planetary-scale cracks [*Leith and McKinnon*, 1996; *Ojakangas and Stevenson*, 1989a; *Geissler et al.*, 1998] suggests that the ice layer may rotate at a different rate than the planetary interior, gliding over an underlying fluid layer. Crater morphology studies [*Schenk*, 2002] find a change in material properties consistent with a solid-liquid interface ~ 20 km beneath the surface. Several features on the surface may represent liquid or semiliquid “cryovolcanic” outflows [*Head et al.*, 1998]. Most of these observations are also consistent with a warm ductile ice layer, but taken together with the magnetic field data, a liquid ocean layer seems to be the most plausible explanation. For the purposes of this paper, we shall assume that a substantial liquid layer does, in fact, exist.

In Europa’s “chaos” regions (of which the Conamara region is the archetype), the original crust appears to have been broken into sharp-edged polygonal blocks; these ice rafts are surrounded by rough-textured, low-lying “matrix” material. The blocks are translated

and rotated from their original orientations. The scene is reminiscent of tabular Antarctic icebergs locked in a matrix of sea ice, but the true formation process is the subject of intense debate [*Greenberg et al.*, 1999; *Collins et al.*, 2000].

Chaos regions on Europa are rarely found in isolation. In many cases, a large chaos region is surrounded by a large number of small, subcircular bumps or depressions typically 7-11 km in diameter [*Pappalardo et al.*, 1999a; *Spaun et al.*, 1999]. These ‘lenticulae’ have textures and other features which resemble larger chaos regions, leading some [*Greenberg et al.*, 1999; *Spaun et al.*, 2002; *Figueredo et al.*, 2002] to propose that similar processes create both chaos and lenticulae.

Tidal forcing is generally accepted as the most likely source for the heat required to maintain the liquid layer, and to create cryovolcanic features [*Peale*, 1999]. However, in the absence of detailed information about the rheology of Europa’s rocky interior and ice layer, the magnitude of this heating is poorly constrained. However, mean heat fluxes of 25-50 mW/m² and conductive ice layer thicknesses between 10 and 30 km are frequently predicted (see [*Pappalardo et al.*, 1999a], and references therein.)

Two end-member models for the formation of chaos and other localized surface disruptions have emerged. The first [*Collins et al.*, 2000] invokes solid-state convection within the ice shell. In this model, chaos regions form over upwelling ice diapirs; salts within the ice may allow some partial melting to occur [*Head and Pappalardo*, 1999; *Pappalardo et al.*, 1999b].

The second [*Greenberg et al.*, 1999] suggests that chaos regions denote areas where a local heat source has melted entirely through the ice crust. Here, the matrix represents re-frozen water or slush and the blocks are pieces of thicker crust that have broken off and

drifted into the interior of the melted zone. *O'Brien et al.* [2002] describe the melt-through process using a model of conductive heat flux through the ice slab, and melting at its base. However, Goodman, Collins, and Pierrehumbert (“An improved melt-through model for chaos formation on Europa”; submitted to *Icarus*, 2003) present an improved model thermodynamic ice model, which demonstrates that total melt-through is implausible in European circumstances: even for very large local heat sources, a layer of ice tens or hundreds of meters thick remains, insulating the liquid from the cold surface.

The melt-through model relies on a local heat source beneath the ice to drive chaos formation. This heat must be communicated from the rocky interior to the ice layer, through the intervening liquid water layer. The behavior of the water layer strongly affects this heat transport, and imposes its own space and timescales on the delivery. Thus, understanding the fluid dynamics of the ocean layer can help us choose between chaos formation models.

Several authors [*Greenberg et al.*, 1999; *Thomson and Delaney*, 2001; *Collins et al.*, 2000] consider the effect of warm, buoyant hydrothermal plumes, fed by geothermal energy at the base of Europa’s liquid layer, which rise through the ocean layer to warm the base of the ice. This localized heat source might drive the localized disruption seen in chaos regions, by melting partially or completely through the ice layer, or by exciting solid-state convection within the ice itself. Are the physical parameters of hydrothermal plumes (dimensions, time scales, heat fluxes and velocities) consistent with what is known of the chaos regions, or must we seek another explanation for them? Here, we present a representation of hydrothermal plume dynamics on Europa, using theoretical ideas gained by the study of convection in Earth’s ocean. We also show the results of several simple

laboratory experiments designed to pin down unknown scaling constants, and to provide visual demonstrations of plume behavior under Europa-like conditions.

The goals of this study are similar to those of *Thomson and Delaney* [2001], though our approach, results, and conclusions are quite different. In section 2.2, we provide a brief synopsis of their results; in section 4, we discuss the differences between our work and theirs.

2. Previous Work

2.1. Convection in Earth's Oceans

The dynamics of convection in Earth's oceans has been considered for two major phenomena: the ascent of buoyant hydrothermal plumes from a seafloor source [*Helfrich and Battisti*, 1991; *Speer and Marshall*, 1995], and the descent of dense surface water, cooled by the atmosphere during wintertime, into the depths [*Marshall and Schott*, 1999; *Jones and Marshall*, 1993; *Maxworthy and Narimousa*, 1994; *Klinger and Marshall*, 1995; *Visbeck et al.*, 1996; *Jones and Marshall*, 1997; *Whitehead et al.*, 1996]. The dynamics of ascending versus descending plumes are indistinguishable: the key difference between these two phenomena is the size of the buoyancy source. Hydrothermal plumes are generally treated as point sources, arising from a single vent or collection of sources of negligible lateral extent. In the wintertime deep convection problem, buoyancy loss occurs over a much wider area.

The dynamics of both problems are similar: convective fluid mixes as it rises/falls, forming rotating masses of diluted buoyant fluid whose motion and geometry are controlled by Coriolis interactions¹. The column of plume fluid eventually goes baroclinically unstable, ejecting swirling blobs of fluid laterally to maintain a steady-state mass balance

in the convective zone. The width of these ejected eddies is set by the “Rossby radius of deformation”, a scale determined by the ratio of buoyancy forces to the Coriolis effect.

Earth’s ocean is stratified: its density increases significantly with depth. In a stratified fluid, a warm hydrothermal plume rises, mixing with its surroundings, until it reaches a “neutral buoyancy level”, at which its density equals that of the surroundings. At this point, the plume has no net buoyancy, and so spreads laterally [*Thomson et al.*, 1992; *Speer and Marshall*, 1995], forming a mushroom or anvil-shaped plume reminiscent of a thunderstorm. (Indeed, the shape of a thunderstorm is also influenced by convection and ascent to a neutral buoyancy level.)

The hydrothermal plume continues to spread until it grows wider than the Rossby radius of deformation r_D . The Rossby radius is the limiting radius of a stable buoyant plume in a fluid on a rotating planet: if it grows beyond this size, the baroclinic instability process causes it to break up into smaller eddies [*Speer and Marshall*, 1995; *Helfrich and Battisti*, 1991]. These eddies spin away from the plume source. Thus, a steady-state plume can be maintained, whose characteristic radius is r_D , which maintains a balance between geothermal heat supply and export via eddy shedding.

Some laboratory experiments and numerical simulations have also been done on convection in an *unstratified* ambient fluid [*Fernando et al.*, 1998; *Jones and Marshall*, 1993]. This situation is not generally observed in Earth’s oceans, but we will demonstrate that it may be relevant to European ocean dynamics. The overall dynamics of this situation are similar, though now there can be no neutral buoyancy level, so plumes ascend/descend until they strike the top/bottom boundary. This has important consequences for the geometry of the plumes and the scaling laws governing their behavior.

2.2. Hydrothermal Plumes on Europa

Several authors [*Gaidos et al.*, 1999; *Chyba and Phillips*, 2002] have discussed hydrothermal plumes on Europa as possible an energy source for biological activity. The impact of hydrothermal plume heating on the morphology of the ice crust has been discussed informally for years; [*Collins et al.*, 2000] seems to be the first published, quantitative description. *Collins et al.* considered the behavior of a warm plume ascending into an unstratified, nonrotating environment. They noted that since the warm plume tends to mix with its surroundings, its temperature upon reaching the ice/water interface is only a fraction of a millidegree above ambient, and suggested that such a tiny temperature difference would have little effect on the overlying ice.

Thomson and Delaney [2001] (T&D hereafter) provided the first detailed description of how heat can be communicated from hot spots on the surface of Europa's silicate interior, through a liquid layer, to the lower surface of the ice layer. They described how a hot patch of seafloor leads to a buoyant hydrothermal plume. The plume turbulently mixes with ambient fluid, but its width is constrained by Coriolis effects, and may rise to the ice/water interface. They used the existing literature on plumes in a rotating, stratified fluid (i.e., Earth's oceans) to compute the lateral extent and heat flux of the plume at the ice/water interface. They demonstrated that Coriolis effects ignored by *Collins et al.* play an dominant role in determining the structure and scales of the plume.

For their choice of source intensity, T&D find plume widths of $O(10 \text{ km})$ to $O(100 \text{ km})$, in fair agreement with the scales of chaos regions as defined by *Greenberg et al.* [1999]. Their calculations suggest that the heat flux per unit area supplied by the plumes is sufficient to melt through the ice layer (assumed to be 2-5 km thick) in roughly 10^4 years. They

note that, given a steady supply of heat, a hydrothermal plume periodically sheds warm baroclinic eddies into its surroundings, and speculate that the “satellite lenticulae” found near chaos regions may be formed as the warm eddies heat the overlying ice. Finally, they note that ice blocks in Conamara Chaos appear to have drifted in a clockwise direction during chaos formation [*Spaun et al.*, 1998]. They note that this is the expected direction of current flow at the top of a hydrothermal plume at the Chaos’s location. After making an estimate of likely current speeds in the plume, they conclude that the currents could have pushed the blocks into their current orientation if open water existed in the Chaos region for about 22 hours.

Thomson & Delaney’s pioneering work brings an understanding of Earth’s oceans to bear on the European chaos problem, and has inspired us to look more closely at the physical oceanography of European plumes. Our assumptions are very different from theirs; most notably, we assume an unstratified, rather than a weakly stratified fluid (see section 3.1). This leads to significantly different results, discussed in section 4.

3. Hydrothermal Plume Dynamics: Theory and Scaling

In this section, we attempt to find space, time, and velocity scales for a hypothetical hydrothermal plume within Europa’s liquid layer. We derive these quantities using a scaling analysis, which provides an order-of-magnitude estimate, and includes an unknown constant factor of order unity. By fitting these scaling equations to data (both from published experiments and from our own simple experiments) we may find rough empirical values for the unknown factors.

3.1. Stratification

The ascent of warm fluid from a seafloor source can be halted by either the stratification of the ambient fluid or the presence of a solid boundary. As described above, for terrestrial hydrothermal plumes, stratification is the principal impediment. In a stratified fluid, the vertical density gradient determines the Rossby radius r_D , and thus the width of the steady-state plume and the size of eddies shed by this plume (see Section 2.1).

When a solid boundary impedes the ascent, the dynamics are substantially different [Fernando *et al.*, 1998; Jones and Marshall, 1993]. When fluid parcels impinge on a boundary, the fluid is forced to spread out against the underside of the ‘ceiling’ rather than at a neutrally-buoyant level, and the plume fluid remains positively buoyant. Thus, the presence of a barrier affects both the geometry and the buoyancy of the plume. For a neutrally-buoyant plume, the dominant buoyancy contrast is the background vertical density gradient. In a boundary-impinging plume, the dominant contrast is between the ambient fluid and the plume fluid.

Let us consider the overall stratification of Europa’s liquid layer (Figure 1). Earth’s ocean is stratified because it is both heated and cooled at different locations along the upper surface. Water cooled at the poles slides beneath warm tropical water, forming stable stratification. If the dominant source of buoyancy in Europa’s ocean is heat input at the base, the situation is more reminiscent of a pot of water on a stove, or of convection in the Earth’s liquid core². The fluid should be convectively unstable everywhere, and stable stratification should not occur. The heating attempts to place warm water under cold: the warm water rises, mixing turbulently with cold water sinking from above, erasing any vertical temperature gradient. Thus, in the inviscid, nonrotating limit, the stratification

Figure 1

of a fluid heated from below is zero. Nonzero viscosity or rotation [*Julien et al.*, 1996] can lead to a slightly negative stratification.

Salinity variations caused by melting and freezing of Europa's ice might provide an additional buoyancy source at the upper surface of the liquid. This has the potential to produce stable stratification in some locations: we will consider the effect of this buoyancy source in Section 6.

The key assumption of T&D's work is that Europa's ocean was "weakly stratified". The theoretical descriptions of plume dynamics they use [*Turner*, 1973; *Helfrich and Battisti*, 1991; *Lavelle*, 1999] were derived for the case of a stratified fluid: these analyses assume that the ascending fluid can rise to a neutral buoyancy level. In contrast, T&D assumed that the plume encounters the ice/water interface (producing the chaos regions) before it becomes neutrally buoyant. These two assumptions are inconsistent and physically incompatible. The requirement that the plume reach the upper boundary implies that stratification is too weak to control the plume behavior.

T&D's results break down if the stratification of Europa's oceans is zero or slightly negative, as we have argued above. Taken at face value, their equations would predict a maximum plume width which is zero, or takes an imaginary value.

Thus, to understand European hydrothermal plumes, we must turn to the literature describing the ascent of buoyant plumes into an *unstratified, homogeneous* environment [*Fernando et al.*, 1998; *Jones and Marshall*, 1993]. In the rest of this section, we adapt the results of unstratified plume theory to the Europa problem.

3.2. Working Assumptions

In this analysis, we assume that Europa possesses a liquid water layer, and that this layer is unstratified. We assume, based on comparison of gravitational data [*Anderson et al.*, 1998] with geomorphological studies [*Pappalardo et al.*, 1999a], that the thickness H of the ocean layer is ~ 80 km. The conclusions derived below allow for a factor of 2 uncertainty in this value.

We have no data on the heat output F from possible seafloor vent sites. For consistency with T&D's analysis, we assume that the heat flux is similar to that produced by large terrestrial mid-ocean-ridge hydrothermal systems: $F = O(1-10 \text{ GW})$ [*Baker and Massoth*, 1987; *Thomson et al.*, 1992]. We will explore the parameter range between 0.1 and 100 GW, and demonstrate that the plume behavior is very weakly dependent on F .

Below, we develop scaling equations for a buoyant hydrothermal plume arising from a point source. These equations are valid when the diameter of the buoyancy source is smaller than the characteristic width of the plume (l_r , defined below). A similar set of equations have been derived for large, diffuse buoyancy sources [*Jones and Marshall*, 1993].

3.3. Scaling Analysis

The derivation below follows the general scaling analysis technique used by many theoretical studies of convection [*Turner*, 1986; *List*, 1982; *Maxworthy and Narimousa*, 1994; *Jones and Marshall*, 1993; *Fernando et al.*, 1998; *Marshall and Schott*, 1999]. The work of Fernando et al. (henceforth, FCA) is particularly valuable, since it deals specifically with the problem of a point-source plume in an unstratified, rotating environment.

While any effect of the hydrothermal plume on the overlying ice layer results from the steady-state action of the plume over many years, we gain a more natural understanding of the problem by considering the initial transient behavior of the plume. At time $t = 0$, we switch on a point-source of buoyancy, with buoyancy flux B :

$$B = g\Delta\rho/\rho_w\mu$$

where μ is the mass flux, in units of m^3/s : thus, B has units of m^4/s^3 . B is related to the heat flux F :

$$B = \frac{g\alpha}{\rho_w C_{pw}} F \quad (1)$$

Here g is surface gravity, and ρ_w , C_{pw} , and α are the density, heat capacity, and thermal expansion coefficient of seawater, respectively.

3.3.1. Initial Behavior: Free Turbulent Convection.

In the initial period after the buoyancy source is switched on, Coriolis forces caused by planetary rotation are unimportant. Furthermore, the plume is too small to feel the finite depth H of the ocean layer. Thus, the buoyancy source B is the only relevant dimensional external parameter. (See Figure 2a.) We may form a length scale from B and the time t since the plume began:

$$L = (Bt^3)^{-1/4} \quad (2)$$

The plume's current height z above the source, and its width l , are both proportional to this characteristic lengthscale: laboratory experiments [Turner, 1986] confirm that the plume grows upward and outward in a self-similar fashion, forming a conical plume. Turner [1986] reports that the height z and diameter l of the plume are related by:

$$l \approx 0.25z$$

Figure 2

The upward mass flux μ (in m^3/s) of the plume is not conserved: it increases as the plume entrains ambient water. However, B is proportional to the energy flux F , and is thus the same at every height in the plume. μ must be a function of B and z , the only available parameters in the problem. The only dimensionally-consistent choice for μ is:

$$\mu = k_\mu (Bz^5)^{1/3}$$

where k_μ is an empirically-determined constant. From experimental values given by *List* [1982], one may derive a value for k_μ :

$$\mu \approx 0.15(Bz^5)^{1/3}$$

Since the buoyancy flux at any height in the plume is simply the buoyancy anomaly $b = g\Delta\rho/\rho_w$ times the mass flux μ , b must be:

$$b = B/\mu \approx 6.7(B^2z^{-5})^{1/3}$$

This relation for b may be used to find the temperature at a given height within the plume.

3.3.2. The Influence of Rotation: Cylindrical Plumets. Europa rotates about its axis once every 3.55 days, resulting in a Coriolis effect. The strength of the Coriolis ‘force’ is controlled by the Coriolis parameter $f = 2\Omega \sin(\theta)$, where Ω is the angular rotation rate of the planet, and θ is the plume’s latitude [*Gill*, 1982; *Pedlosky*, 1987]. Once the system has evolved for roughly one rotation period ($t \sim f^{-1}$), the influence of Coriolis forces becomes important: both f and B are now important external parameters in the problem. For European plumets in the energy flux range considered here, one may demonstrate that at $t \sim f^{-1}$, the plume’s height is still much less than the ocean depth H . At this time, the characteristic length scale for the height and width of the plume

(using Equation 2) is:

$$l_{\text{rot}} = (Bf^{-3})^{1/4}$$

FCA find that, as the plume’s height and width become larger than l_{rot} , the outward growth of the conical plume ceases. The plume begins to exhibit “Taylor column” [Gill, 1982; Pedlosky, 1987] behavior: Coriolis forces suppress vertical shear, and the flow changes from fully three-dimensional turbulence to quasi-two-dimensional, rotationally-dominated motion. At height h_{c1} , the plume begins to deviate from the behavior described in Section 3.3.1: above height h_{c2} , the plume ascends as a cylinder of constant width l_r (see Figure 2b). From FCA’s experimental data, we find:

$$h_{c1} \approx 5.5(Bf^{-3})^{1/4} \pm 10\%$$

$$h_{c2} \approx 7.6(Bf^{-3})^{1/4} \pm 20\%$$

$$l_r \approx 2.4(Bf^{-3})^{1/4} \pm 15\%$$

Thomson & Delaney also describe the confinement of the plume by Coriolis effects. However, the confinement width described above depends on different parameters than those used by T&D.

These rotationally-constrained cylindrical plumes are essentially identical to those found in studies that use a finite-area source of buoyancy [Jones and Marshall, 1993; Maxworthy and Narimousa, 1994]. There, the dilution of plume water by entrainment ceases to change the plume’s buoyancy and volume flux above the critical height h_c . We expect the same behavior here: above h_c , $\mu = \mu(z = h_c)$ and $b = b(z = h_c)$.

$$\mu_{\text{plume}} \approx 0.15(Bh_c^5)^{1/3} = 3.5(B^3f^{-5})^{1/4}$$

$$b_{\text{plume}} \approx 6.7(B^2h_c^{-5})^{1/3} = 0.30(Bf^5)^{1/4} \quad (3)$$

3.3.3. Natural Rossby Number.

The cylindrical plume continues to rise until it encounters the upper boundary of the ocean. At this point, the total water depth H enters as a new external parameter, and it becomes possible to define a non-dimensional number from the external parameters B , f , and H :

$$h_c/H \sim Ro^* \equiv (Bf^{-3})^{1/4}/H$$

Ro^* , the ‘natural Rossby number’³, measures the ratio of the height at which rotation becomes important to the total height of the fluid. If $Ro^* \ll 1$, the plume is controlled by planetary rotation for most of its ascent. If $Ro^* > 1$, the plume reaches the upper boundary before the effects of rotation are felt. We demonstrate in Section 3.4 that $Ro^* \ll 1$ for hydrothermal plumes on Europa. As defined above, Ro^* is conceptually identical to the natural Rossby number defined for finite-area plumes by *Marshall and Schott* [1999] and *Jones and Marshall* [1993].

The scaling laws described above can be recast in terms of Ro^* , H , and f :

$$h_{c1} \approx 5.5Ro^*H$$

$$h_{c2} \approx 7.6Ro^*H$$

$$l_r \approx 2.4Ro^*H \tag{4}$$

$$\mu_{\text{plume}} \approx 3.5(Ro^*)^3 H^3 f$$

$$b_{\text{plume}} \approx 0.30Ro^*Hf^2$$

3.3.4. Interaction with the Upper Boundary: Baroclinic Cones.

What happens when the rising plume encounters the upper surface? The buoyant fluid must be forced radially outward. FCA’s experiments show that the buoyant fluid spreads

laterally over the entire depth, evolving from a cylinder to a straight-sided cone (see Figure 2c).

The onset of baroclinic instability (Figure 2d) limits the growth of this cone. FCA and others find that the plume becomes unstable when its width l_{cone} is of order r_D , the Rossby radius of deformation. At this point, it breaks up into multiple conical eddies.

$$l_{\text{cone}} \approx k'_l r_D \quad (5)$$

where k'_l is a constant of order unity. Different expressions for r_D are appropriate for different fluid density structures. Here, the ambient fluid is unstratified, and the density contrast is a relatively sharp jump between the warm, light water in the plume and the denser ambient fluid. Thus, we should use the Rossby radius appropriate for a two-layer fluid [*Pedlosky, 1987*]:

$$r_D = \frac{\sqrt{b_{\text{plume}} H}}{f}$$

where b_{plume} is the buoyancy contrast between the plume and its surroundings.

Since the turbulent entrainment in the rising plume generates a range of density anomalies, the transition between plume- and non-plume fluid isn't perfectly sharp. Nevertheless, the density change is substantial, and narrow compared to the ocean depth. A 2-layer approximation is also justified by its success in describing the circulation of Earth's upper ocean, whose density variations are even less sharp than our plumes' [*Pedlosky, 1987*].

Inserting from Equation 4:

$$l_{\text{cone}} = k'_{lc} \frac{\sqrt{0.30 Ro^* H f^2 H}}{f} = k_{lc} \sqrt{Ro^* H}$$

The cone diameter scales like the square root of the natural Rossby number.

It now remains to estimate k_{lc} . Unfortunately, FCA do not report an experimentally-derived value for this constant. In Section 3.5, we perform a series of simple tank experiments, and find a k_{lc} from them.

We may also be interested in the time required for the formation of a baroclinic cone. This is equivalent to the time until baroclinic instability begins. The time to fill a cone is given by the volume of the cone divided by the volume flux into it:

$$\tau_{bc} = V/\mu = (\pi/12)l_{\text{cone}}^2 H/\mu = k_{\tau}(Ro^*)^{-2}f^{-1} \quad (6)$$

We must determine k_{τ} experimentally, as it is not reported by FCA.

We are also interested in the characteristic current velocities of the plume system. The difference in swirl velocity between the top and bottom of the cone can be obtained using the thermal wind relation [Gill, 1982; Pedlosky, 1987]. For a two-layer fluid, this relation states:

$$V_{\text{top}} - V_{\text{bottom}} = b/f \frac{\partial}{\partial r} h$$

where b is the buoyancy in the top layer relative to the bottom, and $\frac{\partial}{\partial r} h$ is the slope of the interface separating the two layers, measured radially from the center of the plume.

In our case,

$$\Delta V \sim \frac{2b_{\text{plume}}H}{fl_{\text{cone}}} \approx k_V(Ro^*)^{1/2}Hf$$

This is the *difference* in the velocities between the two layers. We must have information on pressure gradients near the surface to compute the actual velocities. T&D attempted to find an upper bound on this (see Section 4), but no firm data are available. However, since we expect the fluid to be traveling in opposite directions in the two layers (because angular momentum is conserved as the fluid converges at the bottom and diverges near

the top), ΔV is the maximum possible velocity in either layer; velocities half this are more likely.

In FCA's experiments, the baroclinic eddies that form during baroclinic instability also have sizes comparable to l_{cone} . They are pushed around by currents generated by the convecting plume and by each other: they generally drift away from the source region. We expect that their velocity V_{drift} scales with ΔV , the baroclinic current speed calculated above.

$$\Delta V \sim V_{\text{drift}} \approx k_{\text{drift}}(Ro^*)^{1/2} H f \quad (7)$$

We determine k_{drift} experimentally in Section 3.5.

FCA find that the plume maintains its conical shape and diameter l_{cone} after the initial breakup. It reaches a steady-state balance, where the accumulation of buoyant fluid in the cone is balanced by the periodic ejection of baroclinic eddies. It is this steady-state behavior that has a long-term influence on the overlying ice layer. The crucial parameter is the size of the baroclinic cone, which determines the area over which the plume's heat is delivered. The flow velocity is also needed to test T&D's suggestion that geostrophic currents caused the drift of ice rafts in the Conamara Chaos region.

3.4. Parameter values for Europa

All of the quantities derived above depend only on the Coriolis parameter f , the water depth H , and the hydrothermal buoyancy flux B . The Coriolis parameter f is simple to determine:

$$f = 2\Omega \sin \theta$$

where Ω is the planetary rotation rate, and θ is the latitude. The global average value of $|f|$ is $2\Omega/\pi = 1.3 \cdot 10^{-5} \text{ s}^{-1}$ for Europa. At the latitude of Conamara Chaos⁴ (10° N), $f = 0.71 \cdot 10^{-5} \text{ s}^{-1}$.

We shall assume that Europa’s mean ocean depth is between 50 and 140 km. Gravitational measurements [Anderson *et al.*, 1998] suggest an ice+water layer between 80 and 170 km thick, so ocean depth cannot exceed 170 km. Several of the surface morphology studies reviewed by Pappalardo *et al.* [1999a] indicate an ice layer at least 10-20 km thick; on the other hand, if the geological features do in fact indicate the influence of liquid water (rather than mobile ice), the ice layer must be relatively thin.

The most difficult parameter to estimate is the buoyancy source B . B is related to the heat output from a hydrothermal vent via Equation 1. As stated before, we have no direct data on the heat flux output from a putative European hydrothermal plume. Thus, we shall consider values suggested by previous authors [O’Brien *et al.*, 2002; Thomson and Delaney, 2001], plus a substantial margin: we take $F = 0.1 - 100 \text{ GW}$. For comparison, a large active terrestrial vent system emits on the order of 1-10 GW [Baker and Massoth, 1987; Thomson *et al.*, 1992]. We may now use Equation 1 to obtain a value for B . The thermal expansion coefficient α depends on pressure, temperature, and salinity. For pressures corresponding to the base of a water+ice layer between 60 and 140 km thick, and salinities between 0 and 100 psu (Earth’s oceans average 35 psu), $\alpha = 3 \cdot 10^{-4} \text{ K}^{-1} \pm 30\%$. This uncertainty is small compared to the range of F -values we’ve chosen.

Thus, we predict values of B between 0.01 and $10 \text{ m}^4/\text{s}^3$. With such a wide range, can we say anything about the plume behavior? Yes. Note that the plume parameters derived in Section 3.3 depend on B only through their dependence on the natural Rossby

number Ro^* . Ro^* is proportional to the fourth root of B : therefore, changing B by a factor of 1000 changes Ro^* by only a factor of 5.6. The most interesting parameters, the size and velocity scales of the baroclinic cone (l_{cone} and V), are even less sensitive to B : they depend on $\sqrt{Ro^*}$, which varies by only a factor of 2.4 over a 1000-fold change in B .

Using the parameters above, we expect hydrothermal plumes on Europa to lie within the regime $1/60 < Ro^* < 1/10$.

This parameter regime is amenable to small-scale simulation in the laboratory. For example, a buoyancy source of $4 \text{ cm}^4/\text{s}^3$, released into a tank 30 cm deep, rotating at 1 rad/s, has a $Ro^* = 1/35$. Thus, we can build a scale model of hydrothermal plumes in the laboratory. In the following section, we do so. The goal is to demonstrate the appearance and behavior of Europa-like plumes, to confirm the scaling parameters determined by FCA, and to find best-fit values for the undetermined constants k_{lc} and k_V .

3.5. Tank experiment

The experimental apparatus (Figure 3) consists of a rotating table bearing a transparent cubical tank 50 cm on a side, containing water at $\approx 20^\circ \text{ C}$. The rotation rate was varied between 0.25 and 1.5 rad/s; the water depth was varied between 20 and 40 cm. A reservoir containing dyed, salty water (salinity $25 \pm 1 \text{ psu}$) is suspended over the tank. An injector, fed from the reservoir via a needle valve, permits about $0.23 \pm 0.03 \text{ ml/s}$ of salty water to enter the tank via an orifice 2 mm in diameter, located just beneath the surface.

The denser injected fluid sinks, forming a convective plume. To compare the results of this experiment to that of a warm, rising plume, one should mentally flip the plumes upside down.

Figure 3

The descending plume is visualized using a co-rotating video camera mounted above the tank. A mirror at a 45° angle is used to present an elevation view as well as a plan view to the camera.

This apparatus has several weaknesses. First, the use of a narrow injector nozzle means that the fluid leaves the nozzle with a velocity of a few cm/s. The equations described above assumed a source of buoyancy with no initial momentum. However, scaling analysis (see [List, 1982]) suggests that the initial momentum becomes negligible < 1 cm from the injector. FCA used a recirculatory apparatus to ensure a constant pressure at the injector. Our use of a simple small reservoir requires frequent re-filling during the experiment, causing variations in flow rate. FCA's use of a fluorescent dye illuminated by a sheet of laser light allows the imaging of a 2-d cross-section through the convecting fluid: our technique allows us to image only the silhouette of the entire 3-d plume structure, and introduces background clutter and reflections. Finally, our plan-view images are partly obscured by the support apparatus for the injector. Nevertheless, our technique allows us to illustrate and confirm the predictions of Section 3.3.

Table 1 shows the parameters used for the experiments. Since our analysis in Section 3.3 predicts a lack of sensitivity to changes in B , we explored Ro^* -space by varying H and f .

Table 1

Figure 4 shows the evolution of one experiment, which has a tank depth of 30 cm, rotating to give $f = 2 \text{ s}^{-1}$. This corresponds to $Ro^* = 1/35$. The various structures predicted in Section 3.3 are clearly visible. We see a conical freely-convecting plume at $t = 5$ s in Figure 4a; a cylindrical rotationally-controlled plume at $t = 20$ s in 4b; the expansion of the cylindrical plume into a baroclinic cone at $t = 60$ s in 4c; and the breakup

Figure 4

of the cone into baroclinic eddies at $t = 180$ s in 4d and e. After $t = 180$ s, the conical central plume remains, periodically shedding eddies to maintain a steady-state balance. The eddies gradually fill the tank.

From this series of eight experiments, we measured the height h_c at which the plume changed from a conical to a cylindrical profile (see Figure 2b and Equation 4), the width of the descending cylindrical plume l_r , the time to baroclinic instability τ_{bc} (Equation 6), the width l_{cone} the baroclinic cone at the onset of baroclinic instability (Figure 2c; Equation 5), and the drift velocity of the shed eddies V_{drift} (Equation 7). Error bars represent standard deviation of repeated measurements at different times and/or positions within the plume, as appropriate. No standardized criterion was used to define the somewhat diffuse edge of the plume fluid, though all the measurements were performed by one person to ensure consistency. Eddy drift velocities were found by measuring the change in position of eddy centers between two images taken 10-15 seconds apart. We were not able to measure the current velocities of the eddies and the plume: as discussed in Section 3.3.4, drift velocities and swirl velocities should be similar. This was corroborated by qualitative observation of the movement of small-scale structures in the plumes and of markers scattered on the surface of the water.

We compared the scaling laws derived in Section 3.3 to these measurements, and found the best-fit constants of proportionality k . Figure 5 plots the best-fit scaling laws against the measured data; the best-fit k 's are listed in Table 2.

Figure 5

Table 2

We find that the critical height follows the expected Ro^* scaling law very closely. Our best-fit value for k_h is quite close to that reported by FCA. The width of the cylindrical plume l_r fits the data less perfectly, but is still within 25% of the observations. However,

our experimental data suggest a plume width twice that found by FCA. Since the plume edge is not a sharp boundary, this may be partly due to a different criterion in judging the edge location. Also, FCA's laser-sheet imaging technique images a chord sliced through the cylinder, which may be narrower than the mean diameter; our silhouette technique images the widest cross-section, which may be wider than the mean diameter if the plume is not perfectly cylindrical. Note that a scaling law proportional to $\sqrt{Ro^*}$ would fit the data more accurately; however, we cannot justify such a scaling theoretically.

The time to baroclinic instability quite closely follows a $(Ro^*)^{-2}$ scaling law, with the exception of the experiment at $Ro^* = 1/60$. This experiment demonstrated unusual behavior, described below.

Baroclinic cone width is very close to the $\sqrt{Ro^*}$ scaling, except for the $Ro^* = 1/60$ experiment. Eddy drift velocity is not far from $\sqrt{Ro^*}$ behavior, again except for the $Ro^* = 1/60$ outlier; however, a scaling law proportional to Ro^* would fit the data more closely.

The experiment performed near $Ro^* = 1/60$ behaved differently than the others. In this case, the plume never reached the bottom of the tank: instead, it appeared to break up into eddies before striking the bottom. The descending plume was extremely narrow ($l_r \approx 4$ cm across) with most turbulent activity at even smaller scales. At such small scales, molecular diffusivity and viscosity may become important: these factors were considered negligible in the analysis. Viscosity and diffusivity would tend to spread out momentum and buoyancy, increasing the effective width l_r of the plume. A broader plume would have a smaller buoyancy anomaly, and thus a smaller Rossby radius of deformation: this would

reduce the cone width l_{cone} and the time to baroclinic instability τ_{bc} . All these effects match the observed deviation of this experiment from theoretical predictions.

On the whole, we find acceptable agreement between theory and experiment, given the limitations of the apparatus. We may now use these scaling laws to describe hydrothermal plumes on Europa.

3.6. Predicted Scales for European Plumes

3.6.1. Thermal anomaly.

We may roughly estimate the temperature of the plume fluid impinging on the base of the ice layer, using the buoyancy anomaly b_{plume} predicted using Equation 3. The buoyancy anomaly depends only on the heat output and the Coriolis parameter. The thermal anomaly is related to the buoyancy anomaly by the relation $b = g\alpha T'$.

Figure 6 shows the value T' , over the range of plume output power F described in Section 3.4. Despite the wide variation in F of three orders of magnitude, predicted temperature anomalies vary by only a factor of 5. The predicted thermal anomalies are 0.2-1 milliKelvin. This range is much greater the estimate of 0.01 mK estimated by *Collins et al.* [2000], which neglected Coriolis effects; it is much smaller than T&D's estimate of 100 mK. We discuss the reason for this difference in Section 4.3.

Figure 6

While remarkably small, this this temperature anomaly still represents a substantial amount of heat, which must either melt the ice or be conducted through it. And as we shall see, the temperature anomaly is enough to drive measurable currents in and around the plume.

3.6.2. Horizontal scale. Figure 7 uses the scaling equations derived in Section 3 to predict l_{cone} , over the range of H and F described in Section 3.4. Once again, the

Figure 7

parameter is rather insensitive to the wide range of possible values of F : predicted plume width varies by only a factor of 3 over the entire parameter range.

The major conclusion to be drawn from this figure is that the expected equilibrium size of the central plume (25-50 km) is significantly smaller than the size of the Conamara Chaos (75-100 km), and yet quite a bit larger than the size of lenticulae (7-15 km). A comparison of these scales is shown in Figure 8. In the melt-through scenario described by *O'Brien et al.* [2002] (see also [*Greenberg et al.*, 1999]), the size of the melt-thinned patch is always equal to the area over which heating is supplied. Since the lenticulae are several times smaller than the pool of warm water produced by a hydrothermal plume, they are probably formed by a different process. Warm-ice diapirism [*Pappalardo et al.*, 1998] has its own scale-selection properties, and is one possible candidate.

Figure 8

On the other hand, a large hydrothermal plume is the right size to lead to the formation of the entire Conamara Chaos region. As seen in Figure 4e, the eddies shed by the central plume remain in the vicinity for quite some time. The continual formation and ejection of new warm-core eddies supplies a significant amount of warm water out to several times l_{cone} . The warm eddies dissipate as they transfer heat to the base of the ice layer: the distance to which they extend depends on their velocity and the rate of heat transfer into the ice. Inefficient transfer of plume heat to the base of the ice would allow the plume to spread more widely.

3.6.3. Heat Flux. We now estimate the heat flux per unit area (in W/m^2) supplied to the ice by the plume. As stated earlier, without information on the relative efficiency of lateral eddy heat transfer versus vertical conductive transfer, we cannot predict the precise area over which the heat is delivered. However, we have argued that the diameter D of

the heating is probably be somewhat larger than l_{cone} : $D \approx pl_{\text{cone}}$, where $p \gtrsim 1$. Dividing the heat flux by the area of a disk of diameter D gives an estimate of heat flux per unit area.

Figure 9 shows estimates of heat flux per unit area over our chosen range of H and F . For this figure, we have chosen $p = 2$. Uncertainty in p leads to a factor-of-several uncertainty in these flux estimates. As we vary heat output over three orders of magnitude, the area over which the heat is supplied increases by only a factor of 5, resulting in a rather wide range of heat fluxes.

These heat fluxes may be used in a simple thermodynamic model of a conducting ice slab to predict the response of the ice layer to these heat fluxes (Goodman et al., 2003; op cit.). This model predicts that, for the range of heat fluxes shown in Figure 9, a substantial thickness of ice remains unmelted. Thickness is roughly inversely proportional to heat flux, ranging from 2.5 km for a 0.1 W/m² flux to 40 m for a 10 W/m² flux.

3.6.4. Velocities.

Figure 10 shows the predicted eddy drift rates: they range from 3 to 8 mm/s. As we remarked earlier, typical current speeds in the plume region should be similar to these values. Predicted velocities are much slower than the 0.1 m/s estimated by T&D. We discuss the cause and implications of this in Section 4.4

4. Comparison with Thomson & Delaney, 2001

The basic assumptions used in this paper, our techniques, and our results differ significantly from the pioneering work of T&D. In this section, we discuss these differences in detail.

Figure 9

Figure 10

4.1. Stratification and Dynamical Regime of Hydrothermal Plumes

As discussed in Section 3.1, we assume that the plume is governed by the dynamics of convection into an *unstratified* ambient fluid. In contrast, T&D assumed that Europa's oceans were 'weakly stratified', by which they meant that the behavior was governed by the dynamics of convection in a stratified fluid, yet the stratification did not prevent the plume from rising through the entire depth of the ocean.

We noted that T&D's assumption is self-contradictory: if stratification is too weak to halt the ascent of plume fluid to the top of the water layer, then it is inconsistent to assume that the ambient stratification orchestrates the dynamics. The density contrast between plume and ambient fluid is greater than the ambient stratification, a situation more consistent with the unstratified dynamics we use here.

We also justify our assumption of zero stratification by noting that Europa's ocean is heated from below: in such cases, turbulent mixing erases the density gradient utterly.

T&D's assumption of weak stratification allows them to put an upper bound on the strength of stratification within the ocean: stratification greater than this limit would prevent the plumes from reaching the ice. However, they cannot compute a lower bound. Thus, their calculations of plume diameter, thermal anomaly, and heat flux, which depend on the stratification, also only provide upper/lower bounds, though this is not always obvious in their discussion.

4.2. Plume Shape and Evolution

Both our study and T&D's describe a critical height at which the ascending plume fluid's motion becomes dominated by Coriolis effects. Both demonstrate that rotation restricts the radial expansion of the plume. Both agree that, once the plume strikes the

base of the ice layer, it must spread laterally despite Coriolis influences. We concur that the Rossby radius of deformation r_D sets the maximum diameter of the plume; as it grows larger than r_D , it breaks up into baroclinic eddies.

While qualitatively similar, the descriptions differ in detail. In describing the lateral spread of the plume, T&D portray a shallow lens of fluid spreading within the uppermost portion of the ocean (see their Figure 3b), with the bulk of the plume remaining narrow and cylindrical: their diagram portrays the plume forming a ‘trumpet bell’ shape. In contrast, our tank experiments and those of FCA demonstrate that the plume spreads at all depths, swelling to form an inverted cone.

While we agree that the Rossby radius of deformation controls the final width of this cone, our expressions for this radius differ due to our differing assumptions. T&D use an expression valid for a stratified fluid (their Equation 7): it depends on the ambient stratification, ocean depth, and rotation rate, but *not* on the strength of the buoyancy source. Our expression is correct for a ‘two-layer’ fluid: it depends on the buoyancy contrast between the plume and its surroundings, and thus on the strength of the source, but not on the ambient stratification.

If the ambient stratification is zero, as we have argued, then T&D’s expression predicts a maximum plume width equal to zero, a physically unrealistic result. Thus, a different dynamical balance than that assumed by T&D must take over in the limit of weak stratification.

If one takes T&D’s approach, and additionally assumes that the plume reaches a neutral buoyancy level in their stratified fluid at the precise moment that it comes in contact with the base of the ice, then the plume width would be equal to the upper-bound value they

calculated, and would also roughly equal our prediction. However, there is no reason to expect that this special case actually occurs.

4.3. Thermal anomalies under the ice

T&D present a calculation of the thermal anomaly of the plume fluid that impinges on the base of the ice. Their Equation (12) describes the temperature change in a fixed cylindrical volume of fluid heated by the hydrothermal source:

$$\Delta T = \frac{1}{\rho_w C_{pw} \pi r_D^2 d_\tau} \int_\tau F dt$$

where F is the heat source amplitude, τ is the time since the heat source was switched on, ρ_w and C_{pw} are the density and heat capacity of water, r_D is the radius of the cylindrical volume (equal to the Rossby radius of deformation), and d_τ is the thickness of the cylinder. To derive this equation from the definition of heat capacity, one must assume that r_D and d_τ are constant in time. They compute d_τ by supposing that the cylinder is gradually filled by accumulating plume water, so that its thickness at any time is:

$$d_\tau = \left(\frac{r_0}{r_D} \right)^2 \int_\tau w_0 dt$$

where r_0 and w_0 are the radius of the fluid source and the vertical velocity of the fluid it emits.

Note the inconsistency in these equations: the first assumes that the plume's heat increases the temperature of a fixed volume of fluid. The second assumes that the plume's heat increases the volume of fluid at constant temperature. These assumptions cannot simultaneously be true. Taken together, the above equations would imply that in a bathtub filling with warm water, the steady flow of heat from the faucet would eventually cause the water in the tub to boil!

The equation for d_τ is, in any case, incorrect: it assumes that the volume flux at the top of the plume is equal to the volume emitted by the sources at the bottom. Since the warm plume fluid mixes with and turbulently entrains ambient fluid as it rises, the volume flux at the top is many times the flux at the bottom [Turner, 1986].

Our estimate of the temperature of the plume fluid at the ice/water interface emerges from the scaling laws for the final buoyancy of the plume fluid, which is set by turbulent mixing with the less buoyant ambient fluid. Since Coriolis effects act to inhibit this mixing, our estimate is 1-2 orders of magnitude greater than that of Collins *et al.* [2000]. It is 2-3 orders of magnitude less than T&D's.

4.4. Surface current velocity

T&D astutely observe that as warm fluid rises, encounters the ice/water interface, and spreads outward, Coriolis forces produce an anticyclonic swirling motion: clockwise in the northern hemisphere, counterclockwise in the south. Spaun *et al.* [1998] observed that the ice rafts in Conamara Chaos appear to have drifted from their original positions by several kilometers. By reassembling the rafts in jigsaw-puzzle fashion, Spaun *et al.* were able to infer the direction of the rafts' drift. Spaun *et al.* report a clockwise sense of revolution of the field of rafts: T&D note that this is consistent with currents generated by a hydrothermal plume system at Conamara's location. They suggest that the rafts have been pushed into their present position by ocean currents during a melt-through episode.

However, Spaun *et al.* give no error analysis for their drift vectors. Many of the largest drift vectors are badly constrained along the east-west axis: the evidence for circular motion is rather ambiguous⁵. (N. Spaun and G. C. Collins; personal communication,

2002.) Also, there is no tendency for individual blocks to rotate clockwise, as rafts freely drifting in a fluid with clockwise vorticity ought to do.

But suppose we take Spaun’s drift directions at face value. Could ocean currents push the ice rafts to their new locations in a reasonable amount of time?

T&D attempt to estimate the surface current speed within the anticyclonic vortex. By balancing centripetal and coriolis accelerations against pressure gradients caused by a sloping ocean free surface, they compute a maximum possible speed for anticyclonic vortex flow. This value turns out to be 0.1 m/s for a vortex the size of Conamara Chaos.

However, this upper speed limit is rarely reached by geophysical flows. The ratio of flow speed to the above speed limit, $\epsilon = u/u_{\max}$, is equivalent to the “Rossby number” [Holton, 1992]. In large-scale and mesoscale flows in Earth’s atmosphere and oceans, ϵ rarely exceeds 10^{-1} , and is generally much smaller [Gill, 1982; Pedlosky, 1987]. Thus, T&D’s technique leads to a substantial overestimate of plume current speeds.

Our technique makes use of the thermal wind equation, which balances hydrostatic pressure gradients caused by buoyancy variations against Coriolis effects. While this technique is not perfect, it suggests flow velocities of 3-8 mm/s, which is 1-2 orders of magnitude slower than T&D’s estimate.

The weaker currents have important consequences for T&D’s speculations regarding ice-raft drift. Assuming the apparent displacement of ice blocks in Conamara Chaos is a result of advection by plume currents, T&D computed the length of time the ice blocks would need to be mobile to drift as far as observed (8 km). Using their current speed value (0.1 m/s), they find that the ice rafts must have been free to drift for 22 hours.

Using our revised velocities, we find that 2 weeks to a month are required to move the blocks.

This calculation assumes that the ice blocks are completely free to drift with the current, and that they begin to drift at the current speed as soon as they become mobile. In reality, we have demonstrated (Goodman et al., 2003; op. cit.) that melt-through can never be total: a substantial thickness of frozen material remains surrounding the blocks, impeding their motion. We investigate the force balance on an ice raft in Section 5.

4.5. Satellite Lenticulae

T&D suggest that lenticulae might be formed by heat released by baroclinic eddies that spin off the main convective plume. This can only occur if the eddies remain stationary relative to the ice sheet for long enough to achieve significant melting. Calculations by *O'Brien et al.* [2002], T&D, and ourselves (Goodman et al., 2003; op. cit.) agree that the melting process takes $O(10,000 \text{ yr})$ to occur. Thus, for an eddy to create a lenticula, it must drift no more than one lenticula-diameter in 10,000 years, implying a drift velocity slower than 1 meter per year. As we have demonstrated, eddy drift rates are many orders of magnitude larger than this. Thus, freely-drifting eddies would move away too quickly to form satellite lenticulae. T&D's other hypothesis, that the lenticulae are formed by smaller hydrothermal vent sources in the vicinity of the main vent site, would imply that lenticulae have diameters similar to the width of the hydrothermal plumes that form them. The plume diameters we predict in Section 3.6 are several times larger than the lenticulae.

4.6. Melt-through Timescales

Thomson & Delaney present a calculation of the time required for a hydrothermal plume to melt through Europa’s ice layer. They do this by computing the heat capacity H_{cc} of a slab of ice the size of Conamara Chaos, 2-5 km thick, and then dividing by the heat output of an assumed hydrothermal source:

$$t_{cc} \approx H_{cc}/F_{cc}$$

F_{cc} is computed by dividing an estimate of Europa’s global thermal output by the fraction of planetary area occupied by the Chaos. There are several problems here, both in concept and in execution:

- All the basal heat input is assumed to go into melting ice. No heat is permitted to conduct through the ice slab and escape to space. Our model of melt through (Goodman et al., 2003; op. cit.) demonstrates that thermal conduction is a crucial part of this process, and renders complete melt-through impossible.

- The technique for computing F_{cc} assumes that the heat flux supplied to the chaos (in W/m^2) is the same as the planetary average value. If the chaos represents the influence of a hot spot, the heat flux should be above average. If melt-through occurs for planetary-average heat fluxes, why isn’t the entire surface melted? The answer lies in the neglect of thermal conduction, as described above.

- T&D have neglected a factor of 4 in the planetary-surface-area term in their equation (30) for F_{cc} .

Our description of the turbulent mixing of the plume provides a better estimate of the surplus heat flux per unit area applied to the base of the ice layer in Section 3.6.3. We find (Goodman et al., 2003; op. cit.) that conduction through the ice layer balances the heat input before melt-through occurs, leaving an ice layer between 40 m and 2.5 km thick.

5. Drift of Ice Rafts

We now demonstrate that the drag of ocean currents on ice rafts is insufficient to cause the ice rafts to drift. Suppose, as suggested by *Greenberg et al.* [1999] and T&D, that the ice rafts represent floating ice blocks $O(1 \text{ km})$ thick [*Carr et al.*, 1998], broken off from less-melted crust. We suppose that these blocks are embedded in a matrix of solid ice at least $O(10 \text{ m})$ thick — a lower limit on the thickness of unmeltable ice computed by the thermodynamic ice model described by (Goodman et al., 2003; op. cit.), given the heat flux values predicted in Section 3.6.3.

We shall assume that the matrix material resembles terrestrial sea ice, recognizing that the matrix is probably stiffer due to its colder temperature. Terrestrial sea ice behaves as a plastic material [*Hibler*, 1979; *Overland et al.*, 1998]: its rate of strain is negligible until a critical stress is exerted. Thus, the ice raft cannot drift unless the drag force of the flowing water upon the raft exceeds the yield strength of the surrounding matrix: otherwise, it remains locked in place. The drag force is:

$$F_{\text{drag}} = c_D \rho_w u^2 A_x$$

where c_D is the drag coefficient, a constant of order unity; A_x is the cross-sectional area of the raft, ρ_w is the density of water, and u is the flow velocity. Assuming a cylindrical ice raft 1 km thick and 10 km in diameter, with $u = 5 \text{ mm/s}$ and $c_D \sim 1$, we find that $F_{\text{drag}} \sim 0.25 \cdot 10^6 \text{ N}$. This force is applied as a stress along the raft-matrix interface. For a matrix thickness of 10 m, this interface has an area of $3 \cdot 10^5 \text{ m}^2$, resulting in an average stress along the boundary of 0.8 Pa. At various positions around the boundary, this stress may be compressive, tensile, or shear: the order of magnitude is all that is needed for our purposes.

Numerical models of terrestrial sea ice deformation [Hibler, 1979] use a yield strength parameter of $O(10^4)$ Pa for sea ice. More recent modeling studies of the drift of giant icebergs in the ice-covered Weddell Sea [Lichey and Hellmer, 2001] find that icebergs are rigidly locked into solid sea ice until stresses exceed a similar value. Cold European ice should be even stronger than terrestrial ice.

Thus, the drag force caused by ocean currents is many orders of magnitude too weak to permit an ice raft to move through the matrix material. Some other force must be responsible for the observed ice motion: the traction of warm, ductile subsurface ice (discussed further in Section 7) is one possibility.

6. Salinity Considerations

Our discussion thus far has assumed that heating via seafloor hydrothermal activity is the only source of buoyancy in the liquid layer. However, hydrated salts are found on Europa's surface [McCord *et al.*, 1998]; this, along with planetary chemical evolution models [Kargel *et al.*, 2000], suggests that the ocean is salty. Salt is not readily incorporated into ice as it freezes: this results in the release of negatively (positively) buoyant fluid as ice forms (melts). We must consider this buoyancy source in our analysis.

If Europa's ocean were in a steady-state balance, with uniform heat output everywhere and no net melting or freezing, there would be no saline buoyancy source. But since the salty brine rejected by freezing sinks to the bottom, while the fresh water formed by melting floats at the ice/water interface, a nonuniform (in space or time) heat output would tend to stratify the ocean; this counteracts the tendency of seafloor geothermal heating to remove stratification.

Brine rejection upon freezing represents a negative buoyancy source at the top of the ocean. This is no different from the negative buoyancy formed by cooling as heat is conducted into the ice; it promotes descending turbulently-mixing plumes and the removal of stratification. However, *melting* ice forms a thin layer of fresh water at the ice-water interface. What happens to this layer? Does it lead to a large-scale stratification of the ocean layer?

Since water contracts as it melts, the buoyant fresh liquid formed by melting a localized patch of ice would be trapped in the melted concavity in the ice. This would prevent lateral outflow of the buoyant meltwater, and limit the surface area over which mixing and diffusion can modify the salinity; only vertical exchanges across the horizontal base of the melt pool need to be considered.

Salt would tend to diffuse from the saline water below into the meltwater above. However, heat diffuses 100 times faster than salt. This leads to the phenomenon of ‘double diffusion’ [*Schmidt*, 1994]. In situations like ours, where cold fresh water lies above warm salty water, the ‘diffusive layering’ phenomenon occurs. Suppose the interface is perturbed downward, so that a cold fresh parcel is surrounded by warm salty water. Heat diffuses into the parcel faster than salt, resulting in a net gain of buoyancy: the parcel thus tends to rise upward, returning to the fresh layer. The transfer of heat (with little transfer of salt) from the lower layer to the upper layer adds buoyancy to the base of the upper layer, driving turbulent Rayleigh-Benard mixing. The same happens in the lower layer as its top is cooled. Thus, the layers become homogenized, and the layer interface is sharpened. This nonintuitive result – that diffusion can lead to a sharpening of gradi-

ents – is well documented in laboratory experiments and observations of Earth’s oceans [*Schmidt, 1994*].

Thus, buoyant fresh fluid would tend to be confined to a narrow zone directly beneath an area undergoing active melting, with a very sharp interface separating it from the denser, unstratified saline fluid beneath. What impact would this have on the behavior of the buoyant hydrothermal plumes considered in this paper? Plumes would experience unstratified conditions in the lower layer as they form and rise. Their buoyancy anomaly would be less than the buoyancy jump across the double-diffusive layer interface, so they would be unable to penetrate it. Therefore, plume fluid must spread outward below the interface – the interface behaves just like a solid boundary, impeding the upward motion of the fluid⁶. Heat would be transferred across the interface and into the melt layer via thermal conduction across a thin boundary layer, just as it would be if the plume directly contacted the ice. Thus, the length and velocity scales predicted in Section 3 remain relevant when salinity changes caused by melting are included.

7. Conclusions

Beginning with the assumption that a ~ 100 km-thick ocean layer lies beneath Europa’s icy crust, we have described the response of the liquid layer to a local seafloor heat source.

Hydrothermal plumes constrained by Coriolis forces can supply focused heating to the base of Europa’s ice shell. *Thomson and Delaney [2001]* have invoked hydrothermal plumes as agents for the formation of lenticulae and chaos on Europa. Using scaling analysis supplemented by laboratory experiments, we have built up a dynamically-consistent picture of the formation and behavior of these plumes.

Over a wide range of plausible ocean thicknesses and plume heat source magnitudes, we predict that equilibrium plume diameters range between 20 and 50 km. This is much larger than the size of Europa's lenticulae: thus, the scales of the lenticulae must be set by some other process. On the other hand, the size of the plume and its associated warm eddies is consistent with the size of large chaos regions such as Conamara.

The heat flux per unit area supplied by a plume to the base of the ice is not well constrained, ranging between 0.1 and 10 W/m². However, fluxes in this range cannot cause complete melt-through of a conducting ice layer. A layer of ice between tens of meters and a kilometer thick always remains unmelted.

Ocean currents induced by the buoyant plume are predicted to be 3-8 mm/s. This flow is too weak to cause the observed drift of ice rafts in the Conamara region: the remaining ice matrix can effectively resist the drag force caused by the flow, causing the rafts to be rigidly locked in place.

In this work, we have not attempted to precisely estimate the magnitude of local or global hydrothermal activity on Europa. We have simply used magnitudes estimated by previous authors [*O'Brien et al.*, 2002; *Thomson and Delaney*, 2001] to enable comparison with their results. We argue in a separate work (Goodman et. al., 2003; op. cit.) that global and local geothermal output may be weaker than estimated by these authors.

Localized melt-through is inadequate to explain the scales of Europa's lenticulae, and the motion of ice rafts in Conamara Chaos. Viscous flow of warm, ductile ice beneath the cold, brittle surface [*Pappalardo et al.*, 1998] is one possible alternative mechanism. Ductile ice flow is quite compatible with hydrothermal plume heating. A small hydrothermal heat source could lead to ice diapirism, as described by *Pappalardo et al.* [1998]. A larger heat

source could thin the ice sheet through melting; the resulting isostatic adjustment would create a pressure gradient that could push viscous ice toward the thin spot. This flow might drive ice-raft motion. *O'Brien et al.* [2002] demonstrated that this flow was too slow to counteract melt-through of the ice layer, but perhaps it could transport ice rafts laterally a few km, accounting for the motion observed by *Spaun et al.* [1998]. We are presently investigating this possibility. A preliminary calculation suggests that in some cases, ice inflow velocities may exceed 250 meters per millennium.

Hydrothermal plumes may be an effective means of locally heating Europa's ice shell. Despite the huge uncertainties in the parameters governing plume behavior, there are fairly strong fluid-dynamical constraints on the plumes, which lead to important insights about the formation processes of chaos and lenticulae on Europa. Further collaboration between the geomorphology and fluid-dynamics communities is necessary to improve our understanding of the interaction of Europa's liquid and solid components. In addition, Europa provides a unique environment in which to test and extend our understanding of geophysical fluid dynamics.

Acknowledgments. The tank experiments were performed at the GFD lab in the department of Earth, Atmospheric, and Planetary Sciences at MIT, with the assistance of Gordon Brown and Dawn Ash. Richard Thompson provided valuable discussion regarding plume dynamics.

Notes

1. Coriolis control of fluid motion does not require flow velocities "in the water-skiing range", as suggested by *Greenberg et al.* [1999]: Earth's ocean currents are dominated by Coriolis forces, and in fact, flow becomes more geostrophic (more strongly Coriolis-controlled) at slower velocities [*Gill*, 1982; *Pedlosky*, 1987].

2. Unlike a pot of water, Coriolis forces play an important role in the convective motion. Unlike the Earth's core, electromagnetic forces are unimportant: note that Jupiter's magnetic field at Europa is 100 times smaller than Earth's intrinsic field [Zimmer and Khurana, 2000]. As a result, induction drag and field-line tension are utterly negligible.[Cowling, 1957]
3. Readers not familiar with fluid dynamics nomenclature beware: this is not the same as the "Rossby radius of deformation" previously discussed.
4. Note that Conamara Chaos may have formed at a different latitude than its current location, if deformation or polar wander of the ice shell has occurred.
5. Many blocks in the south-central part of the chaos were assumed to have originally been part of a ridge aligned E-W. This fixes their original location perpendicular to the ridge, but their position along the ridge remains uncertain.
6. While the interface behaves as a solid boundary with respect to convective heat flux, the momentum flux is different: a solid boundary requires no-slip boundary conditions, while a fluid-fluid interface does not. However, our earlier analysis made no assumptions about the boundary conditions.

References

- Anderson, J. D., G. Schubert, R. A. Jacobson, E. L. Lau, W. B. Moore, and W. L. Sjogren, Europa's differentiated internal structure: Inferences from four Galileo encounters, *Science*, *281*, 2019–2022, 1998.
- Baker, E. T., and G. J. Massoth, Characteristics of hydrothermal plumes from two vent sites on the Juan de Fuca ridge, northeast Pacific, *Earth Planet. Sci. Lett*, *94*, 59–73, 1987.
- Carr, M. H., et al., Evidence for a subsurface ocean on Europa, *Nature*, *391*, 363–365, 1998.
- Chyba, C. F., and C. B. Phillips, Europa as an abode of life, *Origins Life Evol.*, *32*, 47–68, 2002.
- Collins, G. C., J. W. Head, R. T. Pappalardo, and N. A. Spaun, Evaluation of models for the formation of chaotic terrain on Europa, *J. Geophys. Res. - Planets*, *105*, 1709–1716, 2000.

- Cowling, T. G., *Magnetohydrodynamics*, Interscience Tracts on Physics and Astronomy, Interscience Publishers, 1957.
- Fernando, H. J. S., R. Chen, and B. A. Ayotte, Development of a point plume in the presence of background rotation, *Phys. Fluids*, *10*, 2369–2383, 1998.
- Figueredo, P. H., F. C. Chuang, J. Rathbun, R. L. Kirk, and R. Greeley, Geology and origin of europa’s “Mitten” feature (Murias Chaos), *J. Geophys. Res. – Planets*, *107*, art. no. 5026, 2002.
- Gaidos, E. J., K. H. Nealon, and J. L. Kirschvink, Life in ice-covered oceans, *Science*, *284*, 1631–1633, 1999.
- Geissler, P. E., et al., Evidence for non-synchronous rotation of Europa, *Nature*, *391*, 368–370, 1998.
- Gill, A. E., *Atmosphere-Ocean Dynamics*, Academic Press, 1982.
- Greenberg, R., G. V. Hoppa, B. R. Tufts, P. Geissler, and J. Riley, Chaos on Europa, *Icarus*, *141*, 263–286, 1999.
- Head, J. W., and R. T. Pappalardo, Brine mobilization during lithospheric heating on Europa: Implications for formation of chaos terrain, lenticula texture, and color variations, *J. Geophys. Res. – Planets*, *104*, 27,143–27,155, 1999.
- Head, J. W., N. D. Sherman, R. T. Pappalardo, C. Thomas, and R. Greeley, Cryovolcanism on Europa: Evidence for the emplacement of flows and related deposits in the E4 region (5N, 305W) and interpreted eruption conditions, *Lunar Planet. Sci. Conf.*, *XXIX*, abstract 1491, 1998.
- Helfrich, K. R., and T. M. Battisti, Experiments on baroclinic vortex shedding from hydrothermal plumes, *J. Geophys. Res.*, *96*, 12,511–12,518, 1991.

- Hibler, W. D., Dynamic thermodynamic sea ice model, *J. Phys. Ocean.*, *9*, 815–846, 1979.
- Holton, J. R., *An Introduction to Dynamic Meteorology*, Academic Press, 1992.
- Jones, H., and J. Marshall, Convection with rotation in a neutral ocean: A study of open-ocean deep convection, *J. Phys. Ocean.*, *23*, 1009–1039, 1993.
- Jones, H., and J. Marshall, Restratification after deep convection, *J. Phys. Oceanogr.*, *27*, 2276–2287, 1997.
- Julien, K., S. Legg, J. McWilliams, and J. Werne, Rapidly rotating turbulent Rayleigh-Benard convection, *J. Fluid Mech.*, *322*, 243–273, 1996.
- Kargel, J. S., J. Z. Kaye, J. W. Head, G. M. Marion, R. Sassen, J. K. Crowley, O. P. Ballesteros, S. A. Grant, and D. L. Hogenboom, Europa's crust and ocean: Origin, composition, and the prospects for life, *Icarus*, *148*, 226–265, 2000.
- Kivelson, M. G., K. K. Khurana, C. T. Russell, M. Volwerk, R. J. Walker, and C. Zimmer, Galileo magnetometer measurements: A stronger case for a subsurface ocean at Europa, *Science*, *289*, 1340–1343, 2000.
- Klinger, B. A., and J. Marshall, Regimes and scaling laws for rotating deep convection in the ocean, *Dynam. Atmos. Oceans*, *21*, 222–256, 1995.
- Lavelle, J. W., Buoyancy-driven plumes in rotating, stratified cross flows: plume dependence on rotation, turbulent mixing, and cross-flow strength, *J. Geophys. Res – Oceans*, *102*, 3405–3420, 1999.
- Leith, A. C., and W. B. McKinnon, Is there evidence for polar wander on Europa?, *Icarus*, *120*, 387–398, 1996.
- Lichey, C., and H. H. Hellmer, Modeling giant-iceberg drift under the influence of sea ice in the Weddell Sea, Antarctica, *J. Glaciology*, *47*, 452–460, 2001.

- List, E. J., Turbulent jets and plumes, *Ann. Rev. Fluid Mech.*, *14*, 189–212, 1982.
- Marshall, J., and F. Schott, Open ocean convection: observations, models and theory, *Rev. Geophysics*, *37*, 1–64, 1999.
- Maxworthy, T., and S. Narimousa, Unsteady, turbulent convection into a homogeneous, rotating fluid, with oceanographic applications, *J. Phys. Ocean.*, *24*, 865–886, 1994.
- McCord, T. B., et al., Salts on europa’s surface detected by galileo’s near infrared mapping spectrometer, *Science*, *280*, 1242–1245, 1998.
- O’Brien, D. P., P. Geissler, and R. Greenberg, A melt-through model for chaos formation on Europa, *Icarus*, *156*, 152–161, 2002.
- Ojakangas, G. W., and D. J. Stevenson, Polar wander of an ice shell on Europa, *Icarus*, *81*, 242–270, 1989a.
- Overland, J. E., S. L. McNutt, S. Salo, J. Groves, and S. Li, Arctic sea ice as a granular plastic, *J. Geophys. Res.*, *103*, 21,845–21,867, 1998.
- Pappalardo, R., J. W. Head, and the Galileo Imaging Team, Europa: Role of the ductile layer, in *Lunar and Planetary Science XXX*, Lunar and Planetary Institute, 1999b.
- Pappalardo, R., et al., Does Europa have a subsurface ocean? evaluation of the geologic evidence, *J. Geophys. Res. - Planets*, *104*, 24,015–24,056, 1999a.
- Pappalardo, R. T., et al., Geological evidence for solid-state convection in Europa’s ice shell, *Nature*, *391*, 365–368, 1998.
- Peale, S. J., Origin and evolution of the natural satellites, *Annu. Rev. Astron. Astrophys.*, *37*, 533–602, 1999.
- Pedlosky, J., *Geophysical Fluid Dynamics*, Springer-Verlag, 1987.

- Schenk, P. M., Thickness constraints on the icy shells of the Galilean satellites from a comparison of crater shapes, *Nature*, *417*, 419–421, 2002.
- Schmidt, R. W., Double diffusion in oceanography, *Annu. Rev. Fluid Mech.*, *26*, 255–285, 1994.
- Showman, A. P., and R. Malhotra, The Galilean satellites, *Science*, *286*, 77–84, 1999.
- Spaun, N. A., J. W. Head, G. C. Collins, L. M. Prockter, and R. T. Pappalardo, Conamara Chaos region, Europa: Reconstruction of mobile polygonal ice blocks, *Geophys. Res. Lett.*, *25*, 4277–4280, 1998.
- Spaun, N. A., L. M. Prockter, R. T. Pappalardo, J. W. Head, G. C. Collins, A. Antman, and R. Greeley, Spatial distribution of lenticulae and chaos on Europa, in *Lunar and Planetary Science XXX*, Lunar and Planetary Institute, 1999.
- Spaun, N. A., J. W. Head, and R. T. Pappalardo, The spacing distances of chaos and lenticulae on Europa, in *Lunar and Planetary Science XXXIII*, Lunar and Planetary Institute, 2002.
- Speer, K. G., and J. Marshall, The growth of convective plumes at seafloor hot springs, *J. Marine Res.*, *53*, 1025–1057, 1995.
- Thomson, R. E., and J. R. Delaney, Evidence for a weakly stratified European ocean sustained by seafloor heat flux, *J. Geophys. Res.-Planets*, *106*, 12,335–12,365, 2001.
- Thomson, R. E., J. R. Delaney, R. E. McDuff, D. R. Janecky, and J. S. McClain, Physical characteristics of the Endeavour Ridge hydrothermal plume during July 1988, *Earth Planet. Sci. Lett.*, *111*, 141–154, 1992.
- Turner, J. S., *Buoyancy effects in fluids*, Cambridge Univ. Press, 1973.

- Turner, J. S., Turbulent entrainment: the development of the entrainment assumption, and its application to geophysical flows, *J. Fluid Mech.*, *173*, 431–471, 1986.
- Visbeck, M., J. Marshall, and H. Jones, Dynamics of isolated convective regions in the ocean, *J. Phys. Oceanography*, *26*, 1721–1734, 1996.
- Whitehead, J. A., J. Marshall, and G. E. Hufford, Localized convection in rotating stratified fluid, *J. Geophys. Res. – Oceans*, *101*, 25,705–25,721, 1996.
- Zahnle, K., L. Dones, and H. F. Levison, Cratering rates on the Galilean satellites, *Icarus*, *136*, 202–222, 1998.
- Zimmer, C., and K. K. Khuruna, Subsurface oceans on Europa and Callisto: Constraints from Galileo magnetometer observations, *Icarus*, *147*, 329–347, 2000.

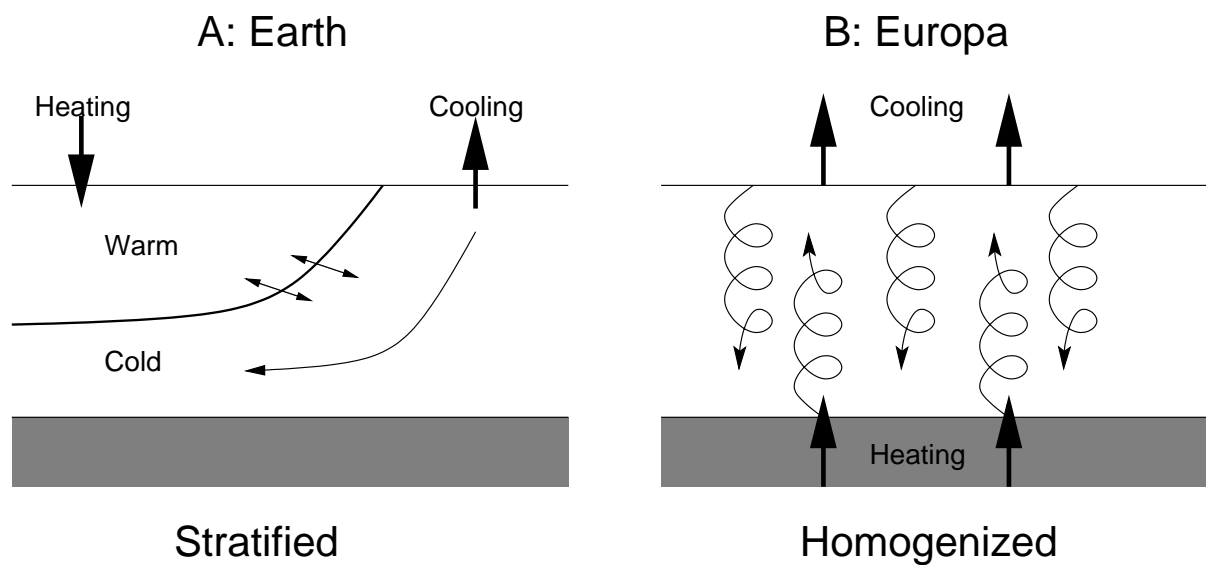


Figure 1. A: Lateral variation in surface heating / cooling allows cool water to slide beneath warm, causing Earth's oceans to become stratified. B: Heating at base, cooling at surface causes instability, turbulent mixing and homogenization of Europa's ocean.

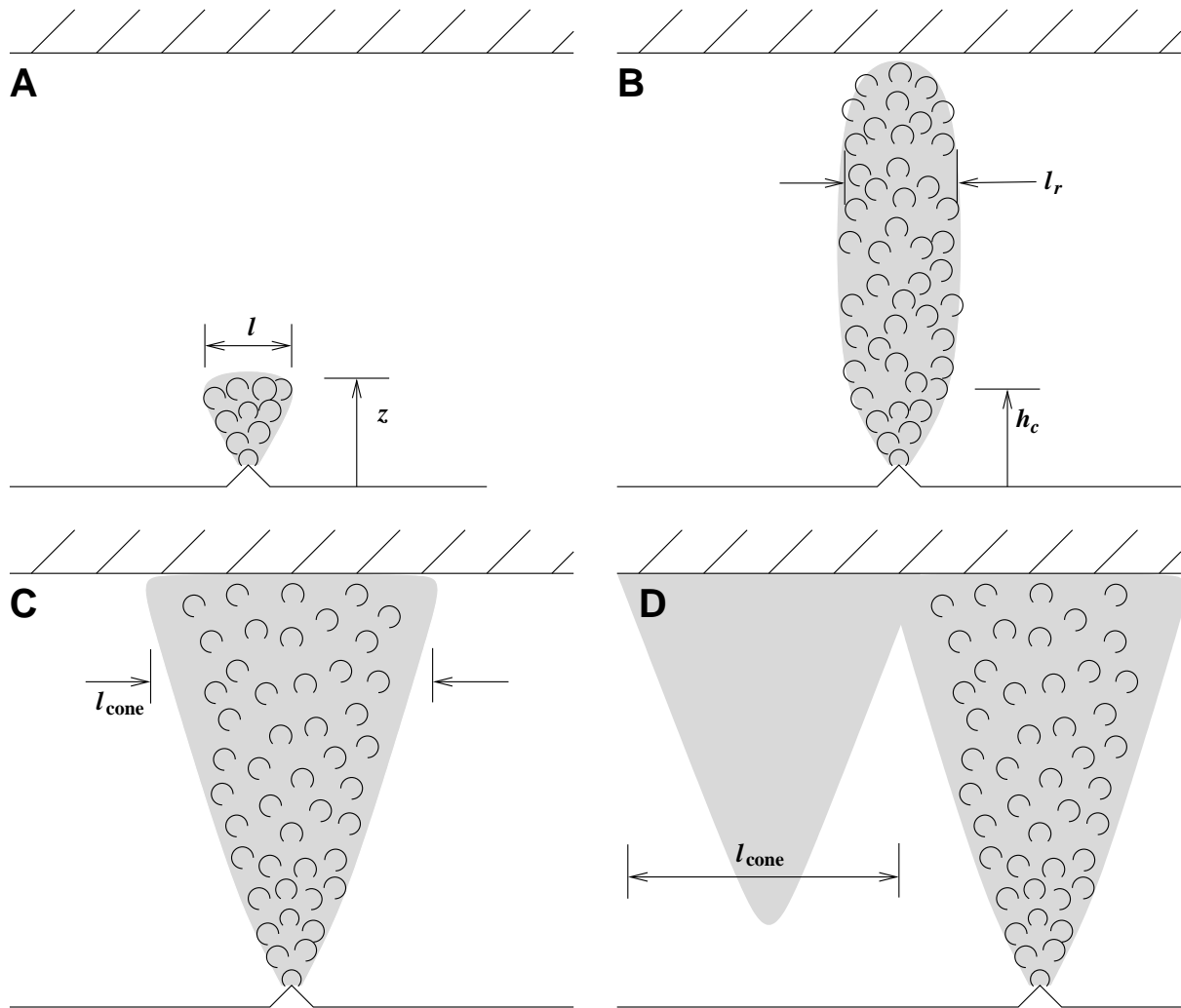


Figure 2. Stages in the evolution of a buoyant convecting plume. See text for full explanation. A: Free turbulent convection. B: rotationally-controlled cylindrical plume. C: Baroclinic cone. D: Baroclinic instability.

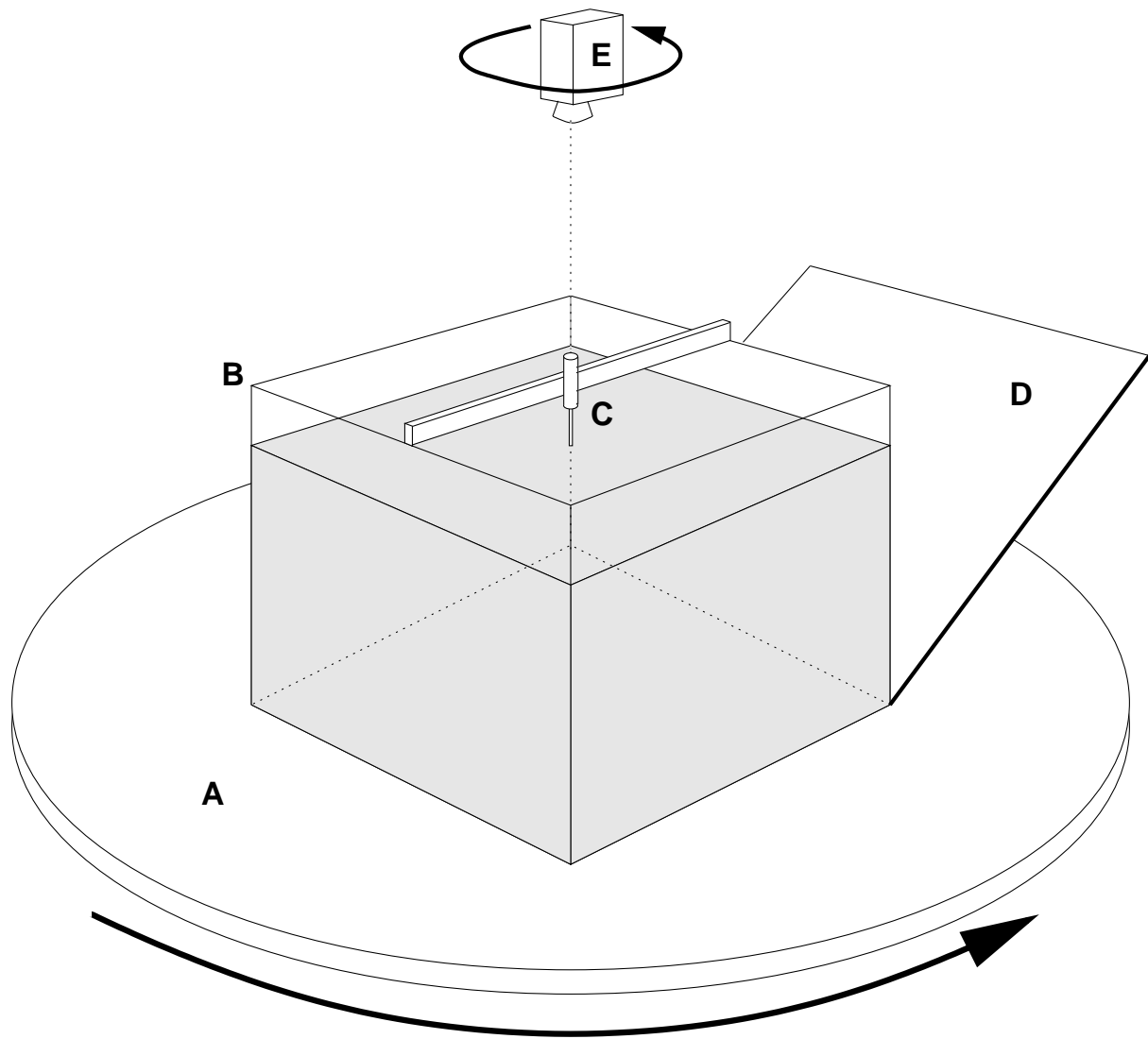


Figure 3. Illustration of experimental apparatus (not to scale). A: Rotating table. B: Lucite tank containing fresh water. C: Reservoir/nozzle apparatus containing dyed saline water. D: Angled mirror to present elevation view to camera. E: Co-rotating video camera.

Experiment #	Vol. Flux (cm ³ /s)	Salinity	B (cm ⁴ /s ³)	H (cm)	f (1/s)	<i>Ro</i> *
1	0.25	25	4.64	30	1	1/20.4
2	0.25	25	4.64	30	1	1/20.4
3	0.23	25	4.27	30	2	1/35.1
4	0.23	25	4.27	30	2	1/35.1
5	0.23	25	4.27	30	0.5	1/12.4
6	0.23	25	4.27	37	3	1/59.0
7	0.23	25	4.27	20	2	1/23.4
8	0.23	25	4.27	20	1	1/13.9

Table 1. Parameter values used in tank experiments.

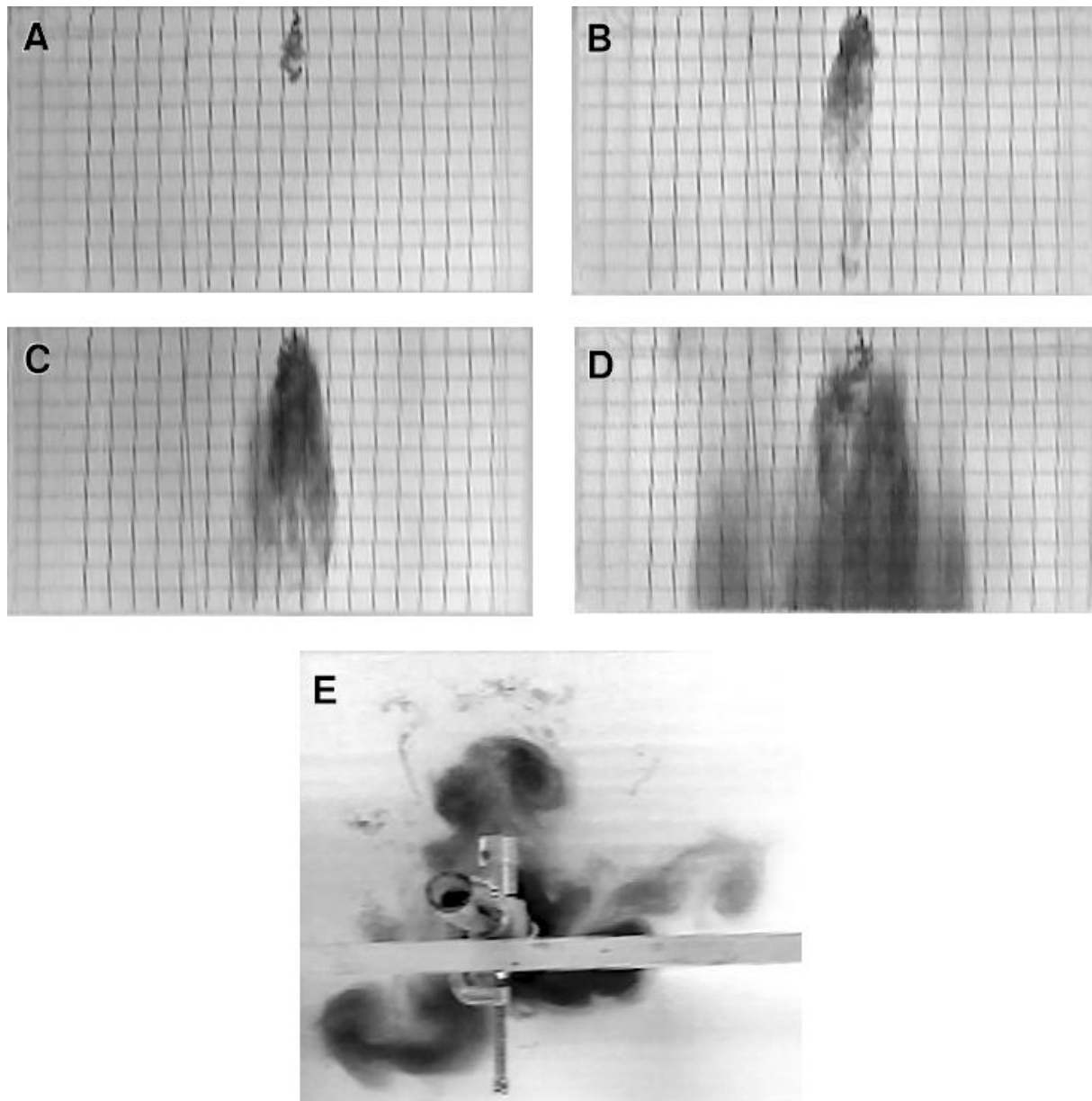


Figure 4. Evolution of rotating tank experiment: $B = 4.3 \text{ cm}^4/\text{s}^3$, $H = 30 \text{ cm}$, $f = 2\text{s}^{-1}$. A: Conical free turbulent convection at $t = 5 \text{ s}$. B: rotationally-controlled cylindrical plume at $t = 20\text{s}$. C: Baroclinic cone at $t = 60 \text{ s}$. D: Eddy-shedding by baroclinic cone at $t = 180 \text{ s}$ (elevation). E: Plan view of eddy-shedding, $t = 180 \text{ s}$. Grid-lines in elevation views are 2.5 cm apart. Flecks of dyed fluid at top of image (E) resulted from a small spill while refilling the injector reservoir.

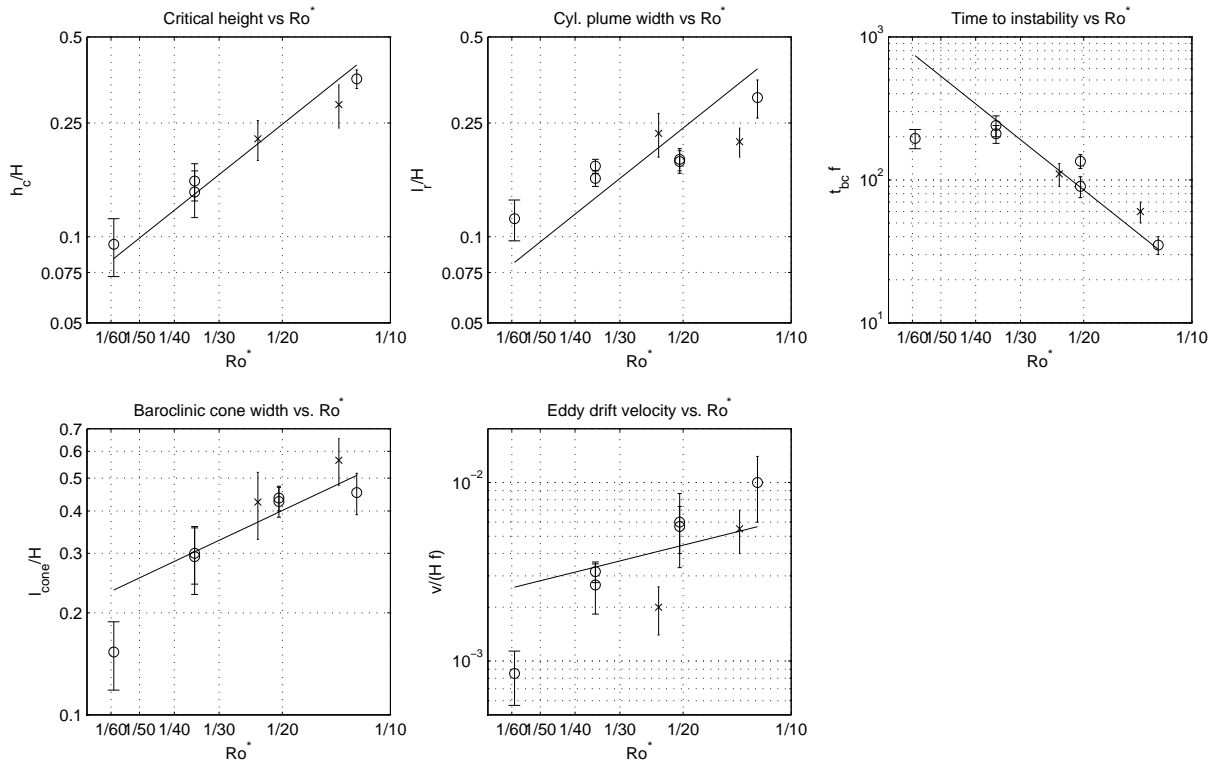


Figure 5. Comparison of experimental parameters with scaling laws. \times 's: experiments with $H = 20$ cm; \circ 's: $H = 30$ or 37 cm. Solid lines show best-fit to scaling laws derived in Section 3.3.

Quantity	Scaling Law	Best-Fit constant	Best-Fit (FCA)
Critical Height	$h_{c1} \approx k_h Ro^* H$	4.95	5.5
Cyl. Plume Width	$l_r \approx k_{lr} Ro^* H$	4.8	2.4
Time to Instability	$\tau_{bc} \approx k_\tau (Ro^*)^{-2} f^{-1}$	0.21	
Cone Width	$l_{cone} \approx k_{lc} \sqrt{Ro^*} H$	1.79	
Drift Velocity	$V_{drift} \approx k_{drift} \sqrt{Ro^*} H f$	0.020	

Table 2. Scaling laws and best-fit constant values for tank experiments. Constant values found by FCA are also reported, where available.

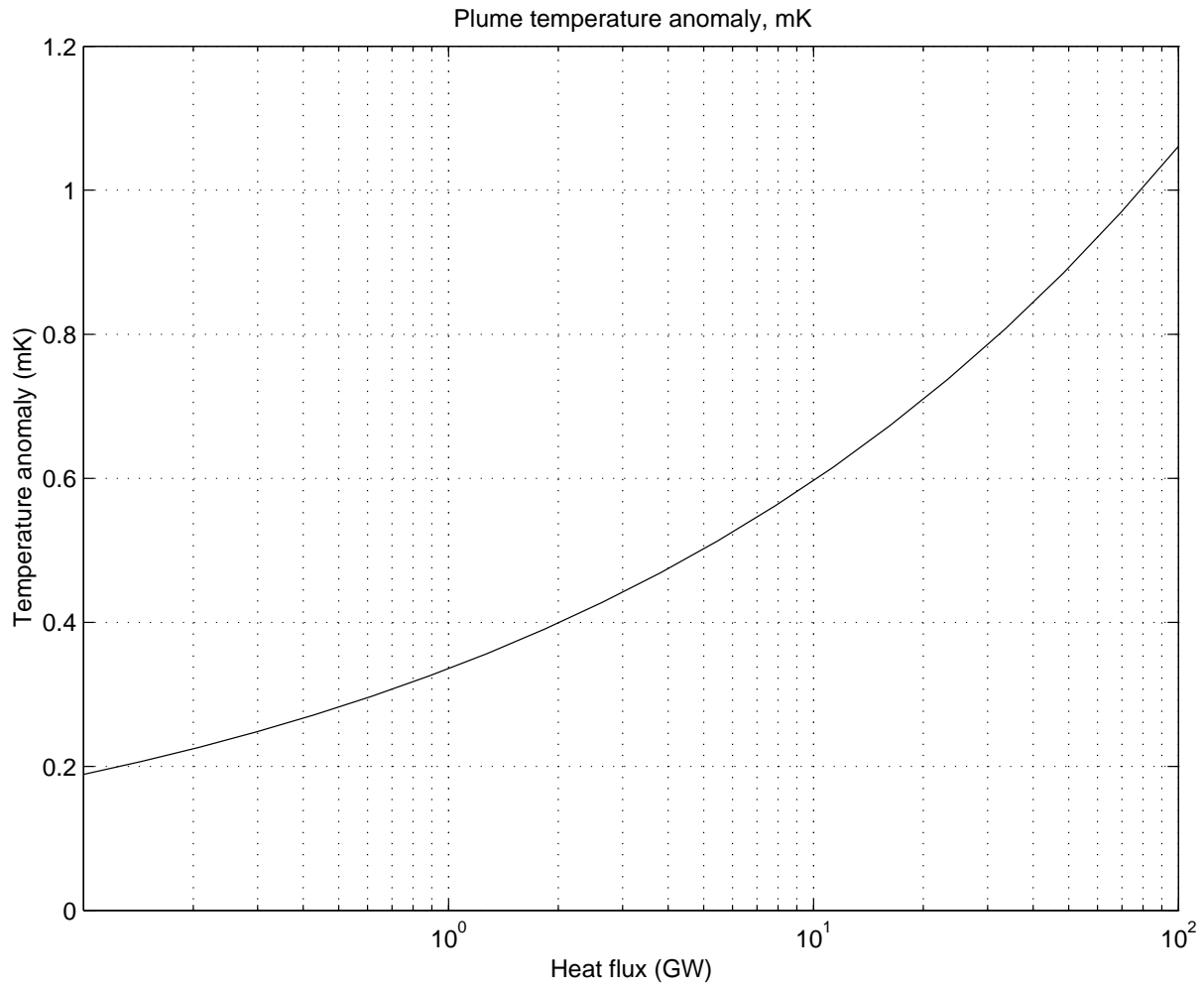


Figure 6. Predicted temperature anomaly of plume fluid, in milliKelvin. Plume output power $F = 0.1 - 100$ GW, coriolis parameter $f = 1.3 \cdot 10^{-5} \text{ s}^{-1}$.

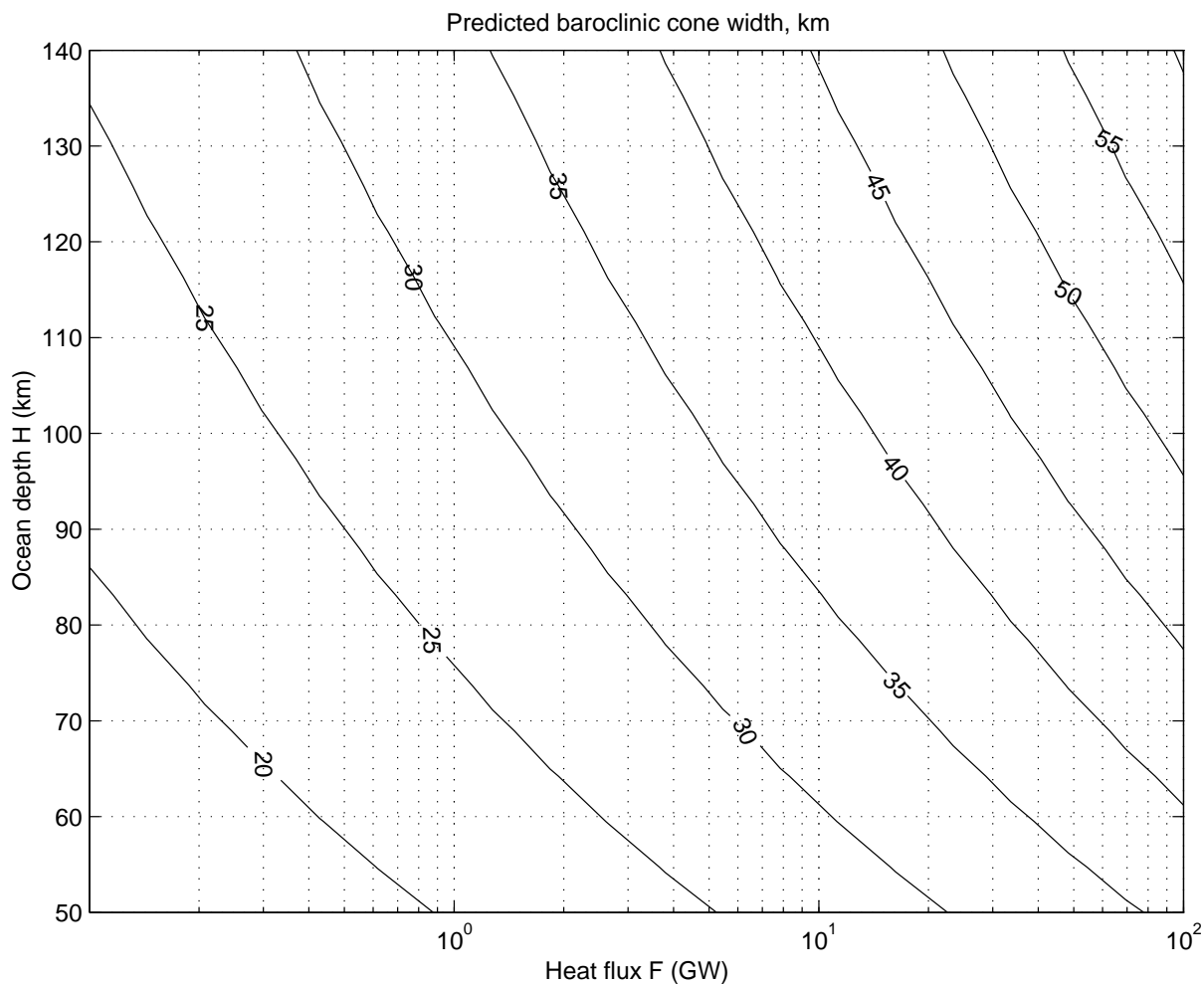


Figure 7. Predicted baroclinic cone width l_{cone} , in km, for hydrothermal plume fluxes $F = 0.1 - 100$ GW, and ocean depths $H = 50 - 140$ km. $f = 1.3 \cdot 10^{-5} \text{ s}^{-1}$.

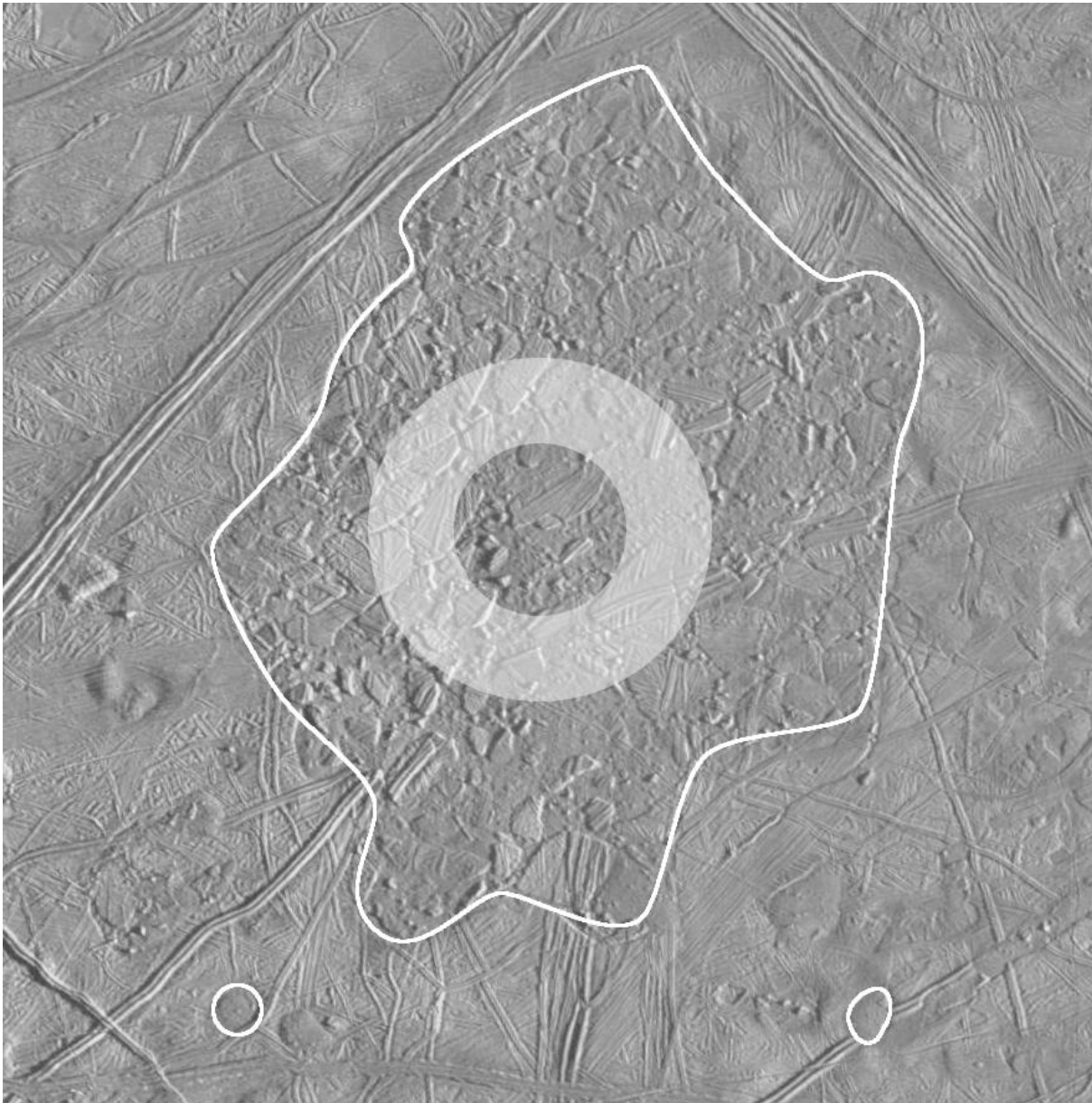


Figure 8. Size comparison of Conamara Chaos and lenticulae with predicted plume diameter l_{cone} . White outlines show approximate boundaries of Conamara Chaos (large irregular outline at center) and of two representative lenticulae (small round outlines at bottom). Shaded circular zone shows range of predicted plume diameters (25-50 km). Base image is from Galileo Orbit E6 imagery.

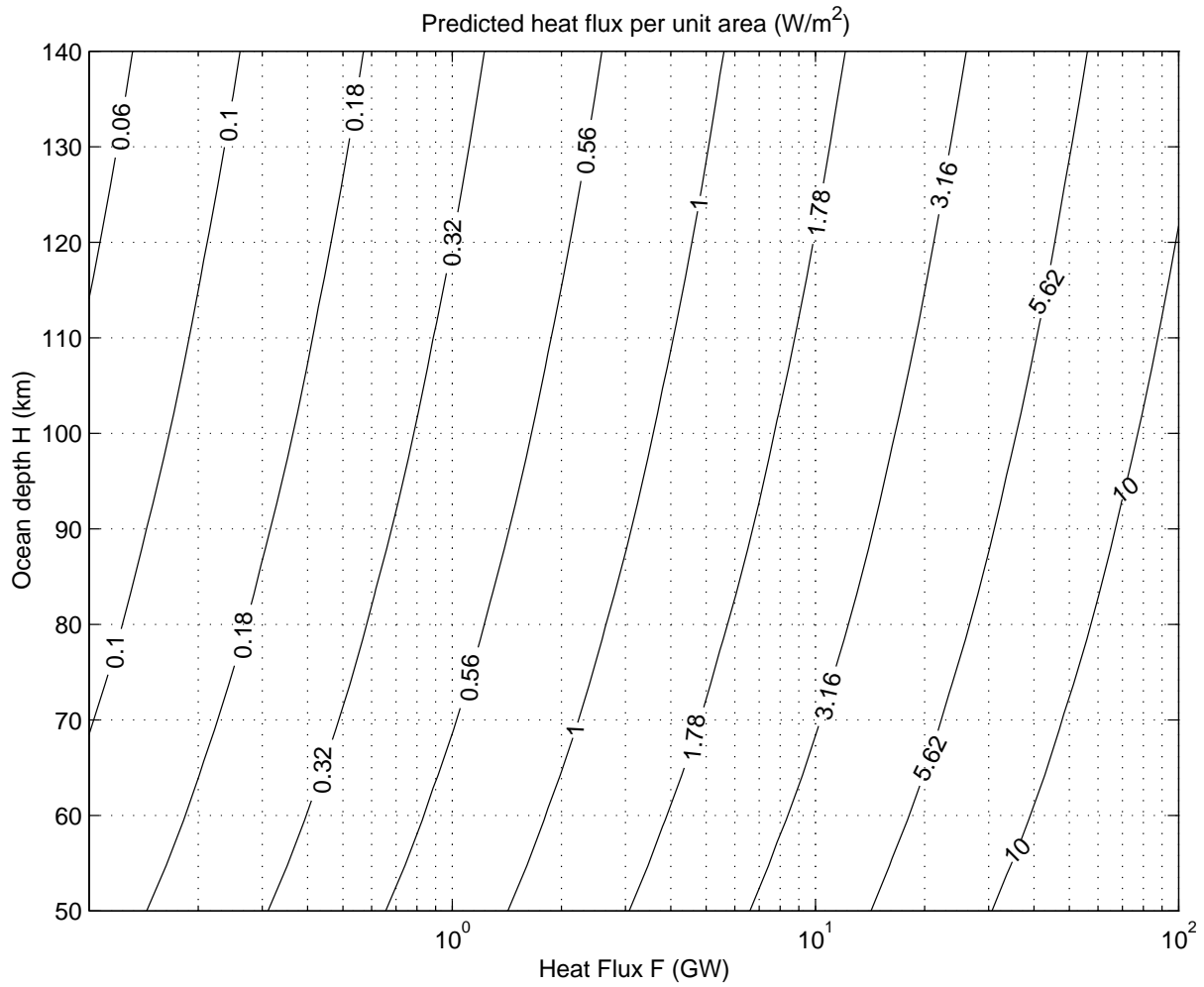


Figure 9. Predicted heat flux (W/m^2) delivered by a plume the the base of the ice layer. over a range of plume output power $F = 0.1 - 100$ GW, and ocean depths $H = 50 - 140$ km. $f = 1.3 \cdot 10^{-5} \text{ s}^{-1}$, $p = 2$.

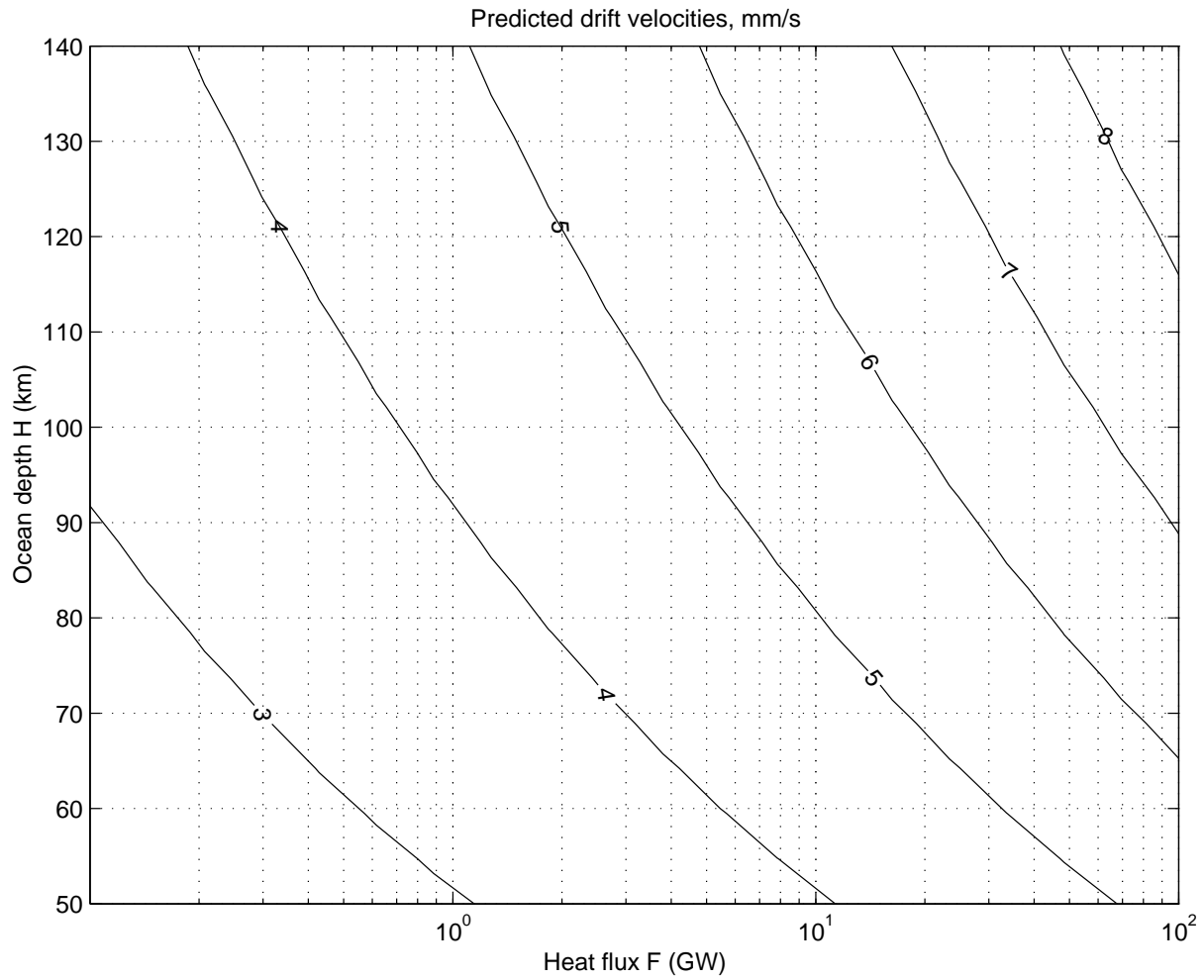


Figure 10. Predicted eddy drift velocities V_{drift} , in mm/s, for hydrothermal plume fluxes $F = 0.1 - 100$ GW, and ocean depths $H = 50 - 140$ km. $f = 1.3 \cdot 10^{-5} \text{ s}^{-1}$.